Wang *et al. Chem Synth* 2023;3:15
DOI: 10.20517/cs.2022.36

Chemical Synthesis

Review

Open Access

Check for updates

Metal-nitrogen-carbon catalysts towards acidic ORR in PEMFC: fundamentals, durability challenges, and improvement strategies

Shuo Wang[1,2,#], Yuyi Chu[1,2,#], Chang Lan[1,2], Changpeng Liu[1,2,*], Junjie Ge[1,2,*], Wei Xing[1,2,3,*]

[1]Laboratory of Advanced Power Sources, Changchun Institute of Applied Chemistry, Chinese Academy of Sciences, Changchun 130022, Jilin, China.
[2]School of Applied Chemistry and Engineering, University of Science and Technology of China, Hefei 230026, Anhui, China.
[3]State Key Laboratory of Electroanalytical Chemistry, Changchun Institute of Applied Chemistry, Chinese Academy of Sciences, Changchun 130022, Jilin, China.
[#]Authors contributed equally.

***Correspondence to:** Prof. Changpeng Liu Laboratory of Advanced Power Sources, Changchun Institute of Applied Chemistry, Renmin Street 5625, Chaoyang District, Changchun 130022, Jilin, China. E-mail: luichp@ciac.ac.cn; Prof. Junjie Ge Laboratory of Advanced Power Sources, Changchun Institute of Applied Chemistry, Renmin Street 5625, Chaoyang District, Changchun 130022, Jilin, China. E-mail: gejj@ciac.ac.cn; Prof. Wei Xing Laboratory of Advanced Power Sources, Changchun Institute of Applied Chemistry, Renmin Street 5625, Chaoyang District, Changchun 130022, Jilin, China. E-mail: xingwei@ciac.ac.cn

How to cite this article: Wang S, Chu Y, Lan C, Liu C, Ge J, Xing W. Metal-nitrogen-carbon catalysts towards acidic ORR in PEMFC: fundamentals, durability challenges, and improvement strategies. *Chem Synth* 2023;3:15. https://dx.doi.org/10.20517/cs.2022.36

Received: 26 Nov 2022 **First Decision**: 29 Jan 2023 **Revised**: 15 Feb 2023 **Accepted**: 6 Mar 2023 **Pulished**: 22 Mar 2023

Academic Editor: Bao-Lian Su **Copy Editor**: Ke-Cui Yang **Production Editor**: Ke-Cui Yang

Abstract

Metal-Nitrogen-Carbon (M-N-C) materials are the most promising Platinum-group-metal (PGM)-free catalysts in replacing the high-cost and scarce Pt catalysts in proton exchange membrane fuel cells (PEMFCs). However, while striking improvement of M-N-C catalysts has been reached in activity, the headache degradation problems hinder their real-world application. Herein, we present a comprehensive overview of the durability of the M-N-C catalyst for oxygen reaction reduction (ORR). The fundamental understanding and identification of the ORR performance of M-N-C catalysts are discussed. Meanwhile, the standard methods to evaluate and predict the ORR performance of the PGM-free catalysts are suggested. We mainly introduce the durability challenges of the M-N-C catalyst and explain the inactivation mechanism in detail. The proposed solution and useful strategies to alleviate catalyst degradation are systematically summarized to overcome the durability bottlenecks.

Keywords: Durability improvement, M-N-C catalysts, ORR, active site

INTRODUCTION

Proton exchange membrane fuel cells (PEMFCs) are promising technologies in the upcoming hydrogen era, which could efficiently convert the chemical energy stored in H_2 into electricity at high efficiency. However, the sluggish oxygen reduction reaction (ORR) process, even on the state-of-the-art Pt-based catalysts at the cathode, has greatly hampered its widespread application[1,2]. Due to costly and scarce Pt catalysts, tremendous efforts have been devoted to lowering the loading of platinum group metal (PGM) by designing PtM alloy or even to completely eliminate its usage by developing new catalyst structures, i.e., developing PGM-free catalysts[3]. The current landscape of PGM-free catalysts encompasses various materials such as M-N-C (Metal-Nitrogen-Carbon) catalysts, carbon-free support catalysts[4], and non-metal catalysts[5]. Among these, M-N-C has exhibited superior ORR performance relative to other PGM-free catalysts[6]. Furthermore, M-N-C catalysts are less expensive and exhibit excellent tolerance to various impurities and organic molecules compared to PGM catalysts[7]. The initial activity of the state-of-the-art M-N-C catalyst is even close to commercial Pt/C and has been revealed as the most promising substitute to replace PGM catalysts[8,9], with a study dating back to 1964 carried out by Jasinski *et al.*[10]. In the following decades, phthalocyanine was used as a precursor to synthesize M-N-C catalysts using a high-temperature pyrolysis procedure. The utilization of Fe-N-C catalysts in fuel cell tests was first carried out by Lefèvre *et al.* in 2009[11]. The catalysts achieved volumetric activity up to 99 A cm^{-3} at 0.8 V, which was a milestone during the development of M-N-C catalysts. In 2011, Proietti *et al.*, by applying Zeolitic-imidazolate-framework (ZIF-8) as the precursor for M-N-C, made a breakthrough in catalytic activity, which even approaches the 2015 US Department of Energy target[12]. Wu *et al.* designed M-N-C (M = Fe, Co) catalysts with outstanding performance with a half-wave potential of only 60 mV lower than commercial Pt/C catalysts in the same year[13]. Recently, the initial activity of M-N-C catalysts was exceedingly advanced, which even approaches the commercial Pt/C catalysts[14,15] [Figure 1].

Fe-N-C catalysts exhibit high ORR activity in acid media but are limited by their poor stability in PEMFC[16]. Fuel cell performances with Fe-N-C cathodes typically degrade by approximately 40% to 80% in the first 100 h of the durability test[12,17]. This phenomenon drives us to reveal the degradation mechanism of PGM-free catalysts. Several mechanisms have been proposed, including demetallation of M-N-C active sites, carbon corrosion, H_2O_2 and active oxygen species (ROS) attacking, protonation of surface N-groups, and water flooding[18,19]. Free radicals produced by the Fenton reaction cause carbon corrosion and demetallation, which is considered as the primary reason for severe active site loss[20,21]. The mechanisms described above are not specific to Fe-N-C catalysts but are also suitable for other M-N-C catalysts. For instance, Co-N-C catalyst exhibited lower reactivity of the Fenton reaction and higher resistance to demetallation[22]. To mitigate catalyst degradation, MN_4 active sites with various metal centers have been investigated. Among these, CoN_4[23], CuN_4[24], CrN_4[25], MnN_4[26], NiN_4[27], *etc.*[28], have demonstrated enhanced stability in comparison to FeN_4. To this end, PGM-free catalysts have been rapidly advanced in the past few years and are now approaching the ultimate application target.

In this review, we first recognize the ORR mechanism and retrospect the identification of active sites of the M-N-C catalyst. Then, we concisely introduce the suggested evaluating and predicting methods of ORR activity and durability on non-precious metal catalysts. After that, we address a systematic discussion of the key stability issues of M-N-C catalyst. Based on the understanding, current strategies for durability improvement of M-N-C catalysts in PEMFC are point-by-point summarized. Finally, we outline the remaining challenges and possible future directions for improving M-N-C catalyst's practicality. Such a

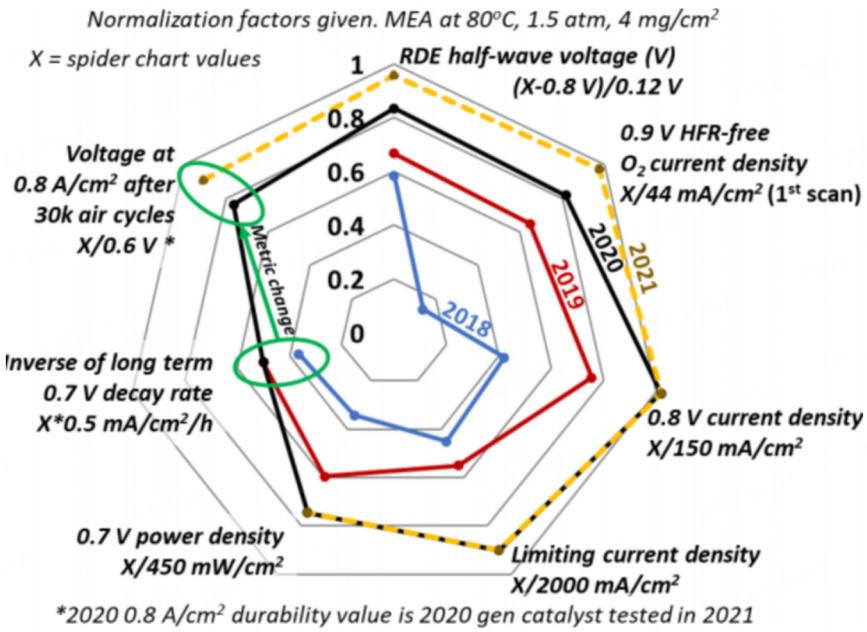

Figure 1. The best metric achieved each year of PGM-free catalysts. This figure is quoted with permission from Litster *et al.*[15].

timely and targeted review will help researchers to grasp the key status of M-N-C catalyst in PEMFC application for guiding future actions.

FUNDAMENTAL OF PGM-FREE ORR ELECTROCATALYSIS

The mechanism of ORR

The ORR mechanism usually includes two pathways in acid media. A direct $4e^-$ pathway O_2 reduction to H_2O, and $2e^- + 2e^-$ pathway O_2 reduction to H_2O_2 which further produces H_2O[29]. The selectivity of the $4e^-$ pathway is an essential parameter for evaluating the performance of catalysts. Currently, our understanding of the ORR mechanism is mainly based on theoretical calculations. The proposed mechanism of ORR can be mainly divided into the following parts:[30-32]

O_2 dissociation:

$$O_2 + * \rightarrow O_2^* \quad (1)$$

$$1/2O_2^* \rightarrow O^* \quad (2)$$

$$O^* + H^+ + e^- \rightarrow OH^* \quad (3)$$

$$OH^* + H^+ + e^- \rightarrow H_2O^* \quad (4)$$

$$H_2O^* \rightarrow H_2O \quad (5)$$

OOH dissociation:

$$O_2^* + H^+ + e^- \rightarrow OOH^* \quad (6)$$

$$OOH^* \rightarrow O^* + OH^* \quad (7)$$

$$O^* + H^+ + e^- \rightarrow OH^* \quad (8)$$

$$OH^* + H^+ + e^- \rightarrow H_2O + * \quad (9)$$

HOOH dissociation:

$$O_2^* + H^+ + e^- \rightarrow OOH^* \quad (10)$$

$$OOH^* + H^+ + e^- \rightarrow HOOH^* \quad (11)$$

$$HOOH^* \rightarrow 2OH^* \quad (12)$$

$$OH^* + H^+ + e^- \rightarrow H_2O + ^* \quad (13)$$

Indirect 4e$^-$ pathway with the yield of H_2O_2:

$$O_2^* + H^+ + e^- \rightarrow OOH^* \quad (14)$$

$$OOH^* + H^+ + e^- \rightarrow H_2O_2^* \quad (15)$$

Multiple ORR intermediates (e.g., O*, OH*, OOH*) involve in ORR, which bind to the surface of catalysts via the O atoms. The rate-limiting step of ORR is determined by the adsorption energy of the ORR intermediates. Too strong binding will hinder the desorption of ORR intermediates, while too weak binding hampers the reaction of the intermediates. Following the Sabatier principle, the catalyst can achieve excellent ORR performance only if the intermediates interact properly with the surface of the catalyst[33-35]. Therefore, adjusting the absorption energy to the optimum value is the process of improving the catalytic activity. The rate-limiting steps and kinetic pathways of ORR remain unclear and are significantly affected by the catalytic site and environment. The pH environment can influence the structure of double layer and further affect the electron transfer process[36]. Pt-based catalysts always exhibited a higher overpotential in alkaline media than in acid media [Figure 2A]. It can be inferred that the Pt surface catalyzes the reduction of 4e$^-$ ORR by chemically adsorbing O_2 in acidic media via an internal spherical electron transfer (ISET) mechanism. However, ORR proceeds through both inner-sphere electron transfer (ISET) and outer-sphere electron transfer (OSET) mechanisms in alkaline media [Figure 2B]. Notably, PGM-free catalysts generally perform better in alkaline media than in acid media, even outperforming Pt/C catalysts sometimes[37]. For PGM-free catalyst, the OSET mechanism is inhibited in alkaline media and the OH adsorption step is different with Pt/C. The OH desorption process of FeN_4 site involves the reduction of (H)O-Fe^{3+}-N_4 to Fe^{2+}-N_4, which facilitates the chemisorption of O_2 and the ISET mechanism. In contrast, the ISET mechanism requires more negative potential due to the lower $Fe^{2+/3+}$ redox potential in acid media. This above mechanism could be used to explain PGM-free catalysts perform better in alkaline media. PGM-free catalysts behave differently in different pH environments and still need further research. Although most PGM-free catalysts have better ORR performance in alkaline media, it is meaningful to develop PGM-free catalysts with high performance in acid media due to the higher maturity of PEMFC than alkaline anion exchange membrane fuel cells[38].

Identification of catalytic active sites

Understanding the structure of active sites of M-N-C catalysts is a prerequisite for designing excellent catalysts. However, synthetic procedures of M-N-C catalyst are usually involved high-temperature pyrolysis of different precursors. The complex Fe-N bond formation process and uncontrolled changes in the carbon matrix during the pyrolysis make it hard to elucidate the formation of active sites. Initially, metal particles encapsulated in carbon shells were regarded as active sites due to the presence of metal nanoparticles observed in many M-N-C catalysts[39]. With the development of advanced characterization techniques, the M-N_x structure is gradually recognized as the actual active site[40]. Lefèvre *et al.* first detected different ions including $FeN_4C_y^+$, $FeN_3C_y^+$, $FeN_2C_y^+$, and $FeN_1C_y^+$ by Time-of-Flight Secondary Ion Mass Spectrometry[41]. Furthermore, Chung *et al.* used high-angle annular dark-field scanning transmission electron microscopy

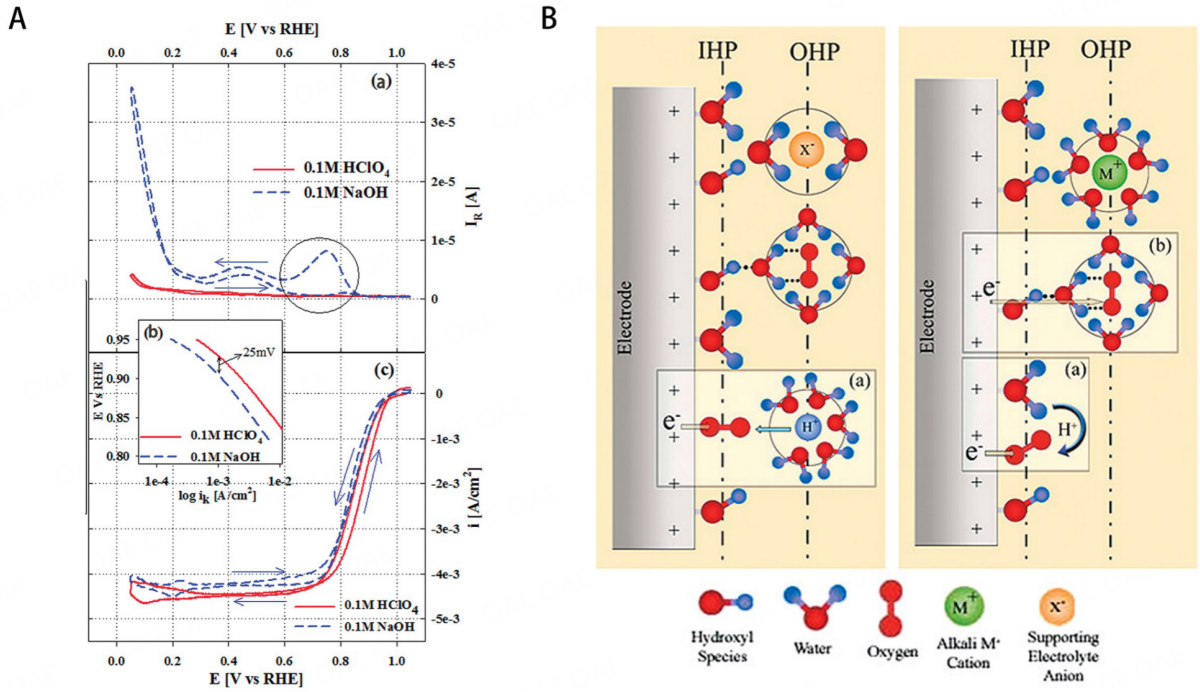

Figure 2. (A) (a) Ring current measured during ORR, (b) Mass transport corrected Tafel plots; (c) ORR polarization curves in O_2 saturated electrolytes; 0.1 M NaOH, and 0.1 M $HClO_4$. (B) Schematic illustration of the double-layer structure during ORR in acidic (left) and alkaline (right) conditions. Insets (a) and (b) illustrate the ISET and OSET processes. These figures are quoted with permission from Ramaswamy *et al.*[36].

(HAADF-STEM) to determine the ratio of Fe and N atoms by the electron energy loss spectrum as 1:4[40], which strongly supported the MN_x structure of active sites. Hitherto several types of active sites can be summarized from previous works, including MN_4, MN_{2+2}, MN_5, M_2N_5, M-N_4/M'N_4, MM'N_6, *etc*[42]. Herein, we take Fe-N-C catalyst as an example to discuss the structure-stability relationship of the active site. Recently, Jaouen *et al.* suggested that Fe-N-C catalysts initially contained two different FeN_x sites of S1 (High-spin FeN_4C_{12} moiety) and S2 (low- or intermediate-spin FeN_4C_{10} moiety) by *in situ* ^{57}Fe Mössbauer spectroscopy [Figure 3A][43]. While S2 sites are stable during long-time Membrane electrode assemblies (MEAs) tests, S1 sites were unstable and easily degraded to ferric oxides. They proposed two possible mechanisms for the formation of ferric oxides. S1 sites of FeN_x can be directly oxidized by O_2 or triggered by protonation of nitrogen and carbon surface oxidation. Following further studies on the structural evolution of the active site, Xu *et al.* used *in situ* ^{57}Fe Mössbauer spectroscopy to reveal the relationship between the oxidized intermediates, the electric field in the electric double layer, and the Fe-N bond strength[44]. They fitted the spectrum into four doublets (note as D1, D2, D3, and D4). D1 was commonly assigned to FeN_4C_8 (low-spin) or FeN_4C_{12} (high-spin) moieties. D2 was most often assigned to FeN_4C_{10} (low or intermediate-spin) moieties. D3 might be attributed to FeN_4 sites coordinating with two weak ligands. D4 might originate from the FeN_4 site that adsorbed oxygen species. As shown in Figure 3B, the demetallation rate of D1 and D2 sites became faster at a high potential which corresponded to the loss of active sites density in the chronoamperometric curve, and half-wave potential in the linear sweep voltammetry (LSV) curve was more significant in relative high potential. The faster loss of D1 than D2 strongly suggested the demetallation influence of the FeN_4 site. The increased content of D4 and the decreased content of D1 and D2 implied that the bare FeN_4 sites could spontaneously adsorb oxygen species to form a five or sixfold-coordinate active center [Figure 3C]. Theoretical calculations demonstrated that both oxidation intermediate adsorption and electric field might lead to longer and less robust Fe-N bonds in FeN_4 sites during ORR [Figure 3D]. On this

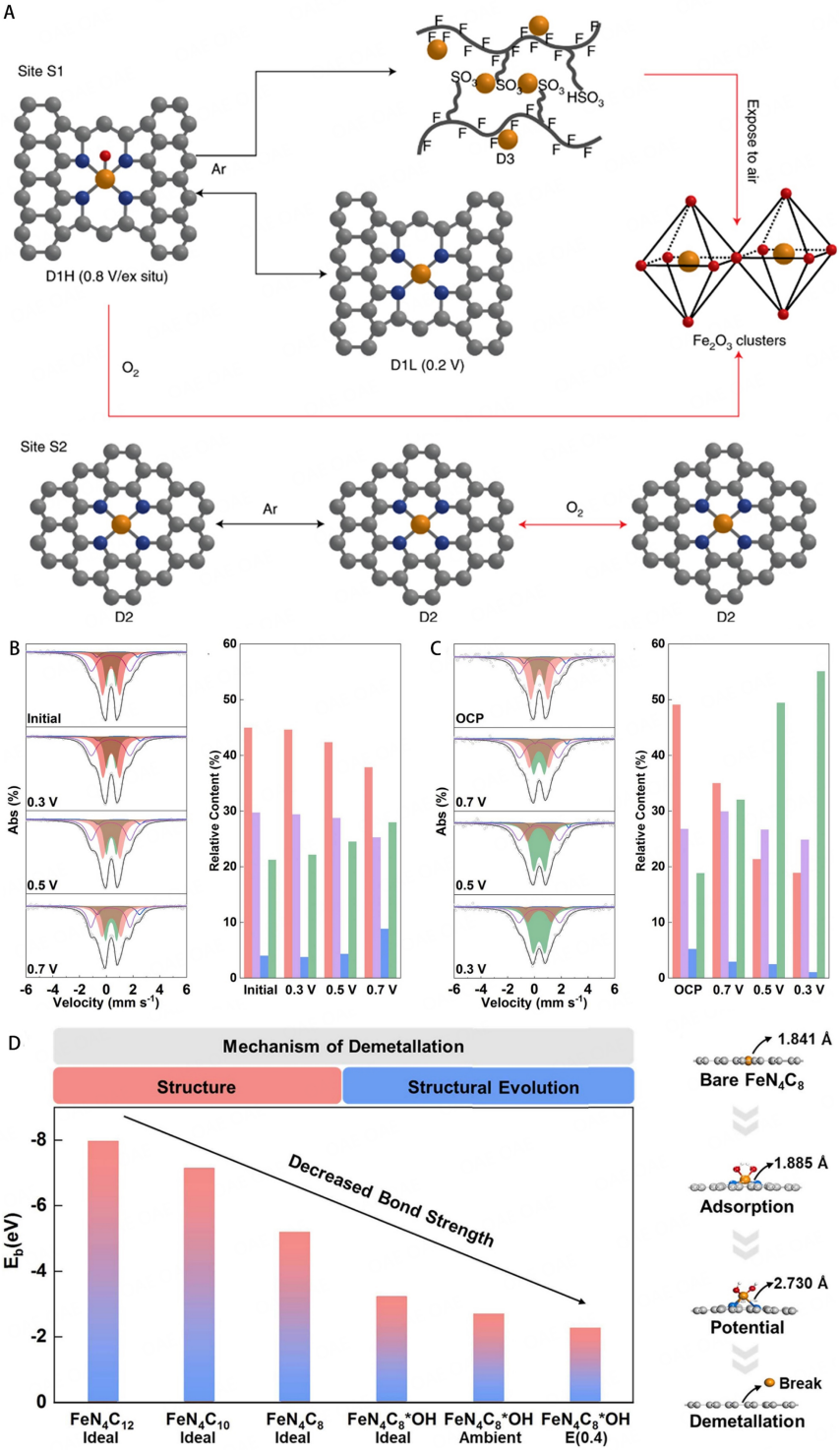

Figure 3. (A) Coordination or structural changes of the S1 and S2 under *in situ* conditions. This figure is quoted with permission from Li *et al.*[43]. (B) The ^{57}Fe Mössbauer spectra on Fe-N-C after degradation at different potentials for 150 h and relative contents of different types of FeN_4. (C) The *in situ* Mössbauer spectra of the ^{57}Fe-N-C and relative contents of different types of FeN_4. (Red: D1; Purple: D2; Blue: D3; Green: D4). (D) The relationship between structural evolution and binding energy or bond length of Fe-N illustrates the bond-breaking process. These figures are quoted with permission from Xu *et al.*[44].

basis, several new directions for improving catalyst durability were found: (1) increase the ratio and density of S2 (or D2) sites; (2) reduce the quantity of S1 or change S1 (or D1) into more stable active sites (S2); and (3) build more robust M-N bonds to reduce the effect of stretched M-N bonds.

Mössbauer spectroscopy is of great importance for the structural analysis of complex Fe-N-C pyrolysis catalysts. However, the complex structure of M-N-C catalyst and limited time-space resolution characterization methods impeded the accurate identification of active moieties. The ^{57}Fe Mössbauer spectroscopy can identify the multiplex composition in Fe-N-C catalysts, but the FeN_x active sites in different oxidation and spin states still lack a theoretical basis to be distinguished[45]. Detailed analysis of various doublets from different Fe structures could not be unambiguously assigned in the experiment due to no reference materials with a single kind of active site. The differentiation of active centers and the degradation of active sites under the ORR condition are still under debate and further insights are promising gained by *in situ* and operando Mössbauer spectroscopy.

In short, the design of M-N-C catalysts with a single type of active site will help to analyze the structure of FeN_4 sites in detail. Advanced *in situ* characterization techniques combined with theoretical calculations are very powerful in predicting active centers and explaining the experimental results.

Methods of evaluating ORR performance

Evaluating the ORR performance of catalysts is an essential part of designing catalysts. Only by acquiring the precise consequence can we well explain the experimental conclusions. However, accurate reflection of intrinsic ORR activity and durability remains a problem. A prevailing issue is that the catalysts exhibit excellent ORR performance in the rotating disk electrode test, but the corresponding MEA performance is still poor. The evaluation methods and test conditions can significantly influence the ORR performance. Here, we concisely discuss common methods for evaluating ORR performance from the ORR activity and ORR durability sections.

ORR activity

Highly active catalysts often suffer severe activity loss after durability testing[46-48]. However, high-durability catalysts usually have poor activity issues. The high activity of the catalysts is the precondition for durability improvement. Achieving both high activity and durability in one catalyst is our ultimate goal for practical applications. Herein, we briefly introduce the different methods for evaluating the ORR activity of catalysts. Rotating disk electrode (RDE) is the most common technique to characterize the ORR performance of the catalysts[49] and the half-wave potential is a key metric for evaluating the ORR activity of PGM-free catalysts[50-54]. The experimental operating parameters would strikingly influence the consequence. Typically, M-N-C catalysts have a catalyst loading of 4 mg/cm^{-2} and a thickness of 100 μm in MEAs. The catalyst loading of M-N-C catalysts ranges from 0.2-0.8 mg/cm^2 in RDE and the thickness (5-20 μm) is similar to the thickness of PGM cathodes in MEAs. The higher catalyst loading usually correlates with higher half-wave potential in RDE test[53]. In contrast, the higher catalysts loading will induce more transport losses in MEA test. Thus, mass activity is also an important metric to evaluate catalytic performance[55-57]. The catalysts loading can also influence the consequence of rotating ring-disk electrode studies. The H_2O_2 produced from the 2-electron pathway can be reduced to water internally rather than at the ring electrode if the electrodes are thick enough[58]. Therefore, it will be more accurate to use mass activity and low loading to characterize the ORR activity and 4-electron selectivity. The electrolyte solution is also a significant parameter for ORR performance testing using RDE. The LSV curve of ORR usually measures with rotating disk electrodes in 0.1 M $HClO_4$ and 0.5 M H_2SO_4 solution. The performance of M-N-C catalysts often rivals or surpasses that of Pt-based catalysts in alkaline solutions. However, their performance remains insufficient in acid

solutions, due to the self-adjustment of FeN_4 sites to *O-FeN_4C in alkaline media[59]. Overall, the universal measurement of the RDE has been identified as simple to investigate the ORR performance of electrocatalysts.

MEAs testing and RDE testing are the most common methods to evaluate electrocatalysts activity. The MEA testing was more complicated than the RDE testing and represented practical fuel cell performances. During the test, RDE can provide a diffusion layer (5-50 μm) to simulate the fuel cell model. MEA is commonly composed of proton exchange membranes (PEM), two catalyst layers (CL), and two gas diffusion layers (GDL). Gas diffusion electrode (GDE) and catalyst coat membrane (CCM) are two typical MEA fabrication processes. Gas diffusion electrode is constructed by depositing catalyst ink on the microporous layer (MPL) of gas diffusion layers. The catalyst coat membrane is formed by depositing the catalyst ink on the membrane[60]. MEA contains a much thicker catalyst layer (5-20 μm), which is hard for mass transportation. Both O_2 and H_2 should pass through the flow fields, gas diffusion layers, and catalyst layers, and finally reach the catalyst surface, which will reduce the concentration of soluble gas (O_2, H_2)[61]. However, RDE has thinner catalyst layers (0.1-2 μm) and shorter diffusion lengths compared with MEA. Therefore, a prevalent problem with ORR catalysts was excellent activity in RDE but poor performance in the MEA testing. Translating catalyst activity and stability into MEA performance remains a challenge and requires further research[52]. Several parameters were used in fuel cell testing to evaluate catalytic performance: (1) the current density at 0.90 V_{iR} in the H_2-O_2 fuel cell reflected the catalytic activity; (2) the current density at 0.80 V expressed the H_2-air fuel cell performance; and (3) high current-density performance in the H_2-air fuel cell in terms of a voltage at 0.8 A cm^{-2}.

Turnover frequency (TOF) and site density (SD) are also essential indexes to evaluate the intrinsic activity of M-N-C catalyst. There are two typical methods to measure SD, including the nitrite stripping technique and the CO chemisorption technique. Primbs *et al.* first developed the *ex situ* CO cryo-adsorption and *in situ* reductive nitrite stripping[62]. A novel relationship was established between SD and structural information of Fe-N-C catalysts. The CO cryo-chemisorption measurement was introduced as follows: six different peak areas (△A) reflecting the amounts of CO absorption were respectively calculated from the six baseline-corrected integral pulse areas after pre-treatment, followed by six CO pluses injected into the sample loop. The calculation formula of △A was as follows:

$$\Delta A = \frac{A_{4,sample}+A_{5,sample}+A_{6,sample}}{3} - \sum_{k=1}^{3} A_{k,sample} \quad (16)$$

A calibration constant c_f was used to convert peak areas to molar CO amounts:

$$N_{CO,ad}[nmol] = c_f \times \Delta A \times 10^6 \quad (17)$$

$$n_{CO}[nmol\ mg_{cat}{}^{-1}] = \frac{N_{CO,ad}}{m_{cat}} \quad (18)$$

The mass-based sites density with CO chemisorption could be calculated via Avogadro's constant (N_A):

$$SD_{mass}(CO)[sites\ mg_{cat}{}^{-1}] = n_{CO}[nmol\ \ mg_{cat}{}^{-1}] \times N_A[site\ mol^{-1}] \times 10^{-6} \quad (19)$$

From the catalyst mass-based kinetic current, TOF could be further calculated.

$$TOF[electron^{-}site^{-1}s^{-1}] = \frac{J_{kin,mass}\times N_A}{SD_{mass}\times F} \quad (20)$$
$$= \frac{J_{kin,mass}\times N_A}{N_{CO,ad}\times m_{cat^{-1}}\times N_A\times 10^{-6}\times F}$$
$$= \frac{J_{kin,mass}}{n_{CO}\times F}$$

Another method was *in situ* reductive nitrite stripping the calculation according to:

$$SD_{mass}(NO_2^{-})[site\ g^{-1}] = \frac{Q_{strip}\times N_A}{n_{strip}\times F\times m_{cat}} \quad (21)$$

$$TOF[electron\ site^{-1}s^{-1}] = \frac{(J_{kin,mass}^{unpoisoned} - J_{kin,mass}^{poisoned})\times N_A}{SD_{mass}(NO_2^{-})\times F} \quad (22)$$

Q_{strip} was coulometric charge in units of coulomb associated with the NO stripping peak; n_{strip} was the number of electrons associated with the reduction of one nitrite ion; m_{cat} was the mass of the catalyst; SD_{mass} (NO_2) was mass-based Fe surface site density. In recent years, Primbs *et al.* reported a novel *in situ* method for SD quantification, which employed a cyanide anion probe[62]. The mechanism was based on the relationship between cyanide-poisoned $Fe^{3+}N_x$ surface sites and decreased ORR activity. Irreversible poisoning of $Fe^{3+}N_x$ sites leads to the reduction in cyanide content, so the active sites could be quantified by ultraviolet–visible spectrophotometry. The linear correlation between cyanide concentration and absorbance supported SD and TOF calculation. It is worth noting that these different kinds of methods may not get the same SD or TOF due to the different adsorption abilities of FeN_x sites. Therefore, we recommend that the same method should be used to compare the TOF values of different catalysts[63].

ORR durability

The durability test with RDE was commonly measured by the loss of half-wave potential after different cycles of the accelerated stress test (AST) (cycling the potentials from 0.6 V to 1.0 V in O_2-saturated 0.5 M H_2SO_4). However, the MEA testing was more accurate than the RDE testing and represented practical fuel cell performances.

Currently, the PGM catalysts durability test was recommended by the US Department of Energy. AST is to cycle the cathode potential from 0.6-0.95 V in a square-wave voltage under the N_2 atmosphere. The activity loss of PGM catalysts matches the loss of surface area; however, the surface area from the double-layer charging current of M-N-C cannot be used to estimate catalytic activity[64]. This is because many other factors will also cause an increase in pseudo-capacitance, such as the increased oxygenated functional groups on the carbon matrix[65]. No apparent discrepancy was observed after changing the cathode gas from N_2 to O_2 during the PGM catalyst durability testing. However, as for M-N-C catalysts, the potential cycle in an inert atmosphere leads to less performance loss than in oxidizing atmosphere[13]. This discrepancy might be attributed to severe carbon corrosion and demetallation caused by ROS. Therefore, the inert gas environment could not induce the same degradation process as PGM-free catalysts in the O_2 atmosphere, which necessitates durability testing of PGM-free catalysts in O_2 or air atmospheres. Zelenay's group reported a test protocol with standardized performance test conditions for durability testing of PGM-free ORR catalysts, which had been approved by the US Department of Energy [Table 1][66]. Herein, we summarized the RDE test [Table 2] and the relevant MEA test [Table 3] results in recent publications.

Methods of predicting ORR performance

Current approaches to designing M-N-C catalysts mainly rely on trial and error, mostly due to the unclear relationship between the structure and performance of ORR catalysts. A theoretical understanding of the

Table 1. MEA test protocol of PGM-free electrocatalyst durability in air and metrics

Test condition	Square-wave cycle in the air: steps between 0.60 V (3 s) and the OCV (but no higher than 0.925 V to minimize carbon corrosion occurring between 0.925 V and 0.95 V) (3 s); a rise time of 0.5 s or less; a single differential cell ≥ 5 cm^{-2}; maintaining a minimum stoichiometry of ~10; a non-stabilized membrane; report fuel cell polarization curve and cathode cyclic voltammetry in N_2 (or another inert gas) at time intervals and conditions specified below	
Total number of cycles	Until the OCV drops below 0.80 V (up to 30,000)	
Cycles time	6 s < t ≤ 7 s	
Temperature	80 °C	
Anode/cathode RH	100%/100%	
Anode gas/cathode gas	H_2/air	
Pressure	100 kPa total partial pressure of N_2 + O_2	
Metric	**Frequency**	**Target**
Catalytic activity	At the beginning and end of the test minimum	≤ 40% loss of initial catalytic activity
H_2-air performance at 0.80 V	After 0, 100, 1,000, 5,000, 10,000 and 30,000 cycles	0.300 A cm^{-2} at the beginning of the test
H_2-air performance at a high current density	After 0, 100, 1,000, 5,000, 10,000 and 30,000 cycles	≤ 30 mV loss at 0.80 A cm^{-2}

This table is cited with permission from Zhang *et al.*[66] published in Nature catalysis.

Table 2. Summary of the RDE and MEA performance of catalysts in recent publications

Catalysts	Active sites	RDE performance			MEA activity
		$E_{1/2}$	Electrolyte	RDE test $\Delta E_{1/2}$	Peak power density
P(AA-MA)(5-1)-Fe-N[67]	FeN_4	0.843 V	0.5 M H_2SO_4	3 mV (5k cycles)	0.65 Wcm^{-2}(H_2- O_2)
surf-FeN_4-HPC[68]	FeN_4	0.83 V	0.1 M $HClO_4$	20 mV (20k cycles)	0.79 Wcm^{-2}(H_2- O_2)
Fe-pyridinic N-C[69]	FeN_4	0.825 V	0.1 M $HClO_4$	21 mV (20k cycles)	-
Co-N-C@F127[70]	CoN_4	0.84 V	0.5 M H_2SO_4	40 mV (30k cycles)	0.87 Wcm^{-2}(H_2- O_2)
Co(mIm)-NC[22]	CoN_4	0.82 V	0.5 M H_2SO_4	8 mV (10k cycles)	0.64 Wcm^{-2}(H_2- O_2)
Co-N-C-10[71]	Co_2N_5	0.79 V	0.1 M $HClO_4$	12 mV (20k cycles)	-
FeSA/FeAC-2DNPC[72]	FeN_4	0.81 V	0.5 M H_2SO_4	15 mV (10k cycles)	0.8 Wcm^{-2}(H_2-O_2)
Cr/N/C-950[25]	CrN_4	0.773 V	0.1 M $HClO_4$	15 mV (20k cycles)	-
17CVD/Fe-N-C-kat[73]	FeN_4	0.835 V	0.5 M H_2SO_4	35 mV (50k cycles)	0.7 Wcm^{-2}(H_2- O_2)
Fe0.5Co@HOMNCP[74]	FeCo	0.903 V	0.1 M KOH	~0 mV (5k cycles)	-
p-FeNC@CoNC[75]	FeN_4-CoN_4	0.87 V	0.5 M H_2SO_4	16 mV (30k cycles)	-
Fe/Zn-N-C[76]	FeN_4-ZnN_4	0.906 V	0.1 M KOH	12 mV (5k cycles)	-
N-Fe_2MoC-GC[77]	FeN_xC, MoN_xC	0.887 V	0.1 M KOH	16 mV (120k cycles)	1.12 Wcm^{-2}(H_2- O_2)
Fe-N-C + Ta-TiOx/KB[78]	FeN_4	0.84 V	0.5 M H_2SO_4	18 mV (10k cycles)	0.7 Wcm^{-2}(H_2- O_2)
NCAG/Fe-Cu[79]	FeN_4, CuN_4	0.94 V	0.1 M KOH	13 mV (8k cycles	-
$FeCoN_X$/C[80]	$FeCoN_5$-OH	0.86 V	0.1 M $HClO_4$	13 mV (5k cycles)	0.819 Wcm^{-2}(H_2-O_2)
Fe-AC-CVD[46]	FeN_4	0.846 V	0.5 M H_2SO_4	17 mV (30k cycles)	0.535 Wcm^{-2}(H_2-air)
Fe-AC[46]	FeN_4	0.915 V	0.5 M H_2SO_4	124 mV (30k cycles)	0.601 Wcm^{-2}(H_2-air)
Feg-NC/Phen[81]	FeN_4	0.84 V	0.1M H_2SO_4	16 mV (5k cycles)	1.53 Wcm^{-2}(H_2-O_2)
Cu/G[82]	CuN_4	0.85 V	0.1 M KOH	10 mV (10k cycles)	-
Cu-SA/N-C[24]	CuN_4	0.895 V	0.1 M KOH	~0 mV (5k cycles)	-
20Mn-NC-second[26]	MnN4	0.8 V	0.5 M H2SO4	17 mV (30k cycles)	0.46 Wcm^{-2}(H_2-O_2)
Sn-N-C[83]	SnN_x	0.73 V	0.1 M $HClO_4$	-	-

ORR catalytic process is a major requirement for rational interpretation of experimental observations and also a prerequisite for rational improving the durability of M-N-C catalysts. Here, we briefly describe the

Table 3. Summary MEA performance of catalysts in recent publications

Catalysts	MEA durability test			
	Test condition	Current density at 0.9 V (H_2-O_2)	Current density at 0.8 V	Voltage at 0.8 A cm^{-2}
target	30k cycles AST	> 44 mA cm^{-2} (H_2-O_2) < 40% loss	> 150 mAcm^{-2} H_2-air	< 30 mV loss
surf-FeN_4-HPC[68]	30k cycles AST	24.2-n/a mA cm^{-2}	87.2-20.9 mA cm^{-2} H_2-air	0.49-0.37 V H_2-O_2
FeSA/FeAC-2DNPC[72]	150 h at 0.5 V H_2/air	15-n/a mA cm^{-2}	85-30 mA cm^{-2} H_2-air	0.42-0.30 V H_2-air
17CVD/Fe-N-C-kat[73]	30k cycles AST	27-n/a mA cm^{-2}	117-64 mA cm^{-2} H_2-air	0.30-0.24 V H_2-air
N-Fe_2MoC-GC[77]	30k cycles H_2/O_2 alkaline fuel	-	650-400 mA cm^{-2} H_2-O_2	0.75-0.72 V H_2-O_2
Fe-N-C + Ta-TiOx/KB[78]	ADT[a]	17-16.5 mA cm^{-2}	106-93 mA cm^{-2} H_2-O_2	0.62-0.57 V H_2-O_2
Fe-AC-CVD[46]	30k cycles AST	33-n/a Ma cm^{-2}	85-55 mA H_2-air	0.48-0.46 V H_2-air

ADT: 20 cycles at 0.85 V for 5 min and 0.40 V for 55 min (duration = 20 h) at 1.0 bar H_2/air at a cell temperature of 80 °C.

current understanding of the relationship between catalyst theory and ORR performance.

ORR activity

The d-band theory was established to combine the surface adsorption strength with the d-state of transition metals. Since all transition metals have similar broad sp-band, the difference in absorption behavior of metal surface is almost determined by the interaction between the d-band states of metals and valance states of adsorbates[84,85]. The d-band center (ε_d) was used to descript the average energy of the d-band and correlated with the adsorption energy and ORR activity. Cao's group presented a design principle to predict the performance of Single-atom catalysts[86]. The free energy of each step is determined by the adsorption energy of the ORR intermediate. They found the linear relationship between electronegativity and the corresponding descriptor (φ) and adsorption energy of ΔG_{OH^*} and ΔG_H*. Higher φ indicates more d-sate valence electrons in the single metal atom. The φ descriptor could be used to predict the adsorption energy of intermediates and catalytic performance.

The free energy diagram of ORR was widely used to predict the rate-determining step. For a classic example, the free energy of 4e$^-$ ORR over Pt is shown in Figure 4A[87]. At U = 1.23 V (equilibrium potential), the positive free energy change (ΔG) of the OH* to H_2O reaction step means that the surface of Pt would be covered by OH* and lose its catalytic activity. The highest potential for a facile reaction process was named thermodynamic limiting potential. The difference between the equilibrium potential and the limiting potential is called the theoretical overpotential (η), which is usually used to measure the activity of catalysts. The lower theoretical overpotential often corresponds to higher catalytic performance[88]. Therefore, the adsorption energy regulation of ORR intermediates was a key to rationally designing highly active catalysts. Similarly, the volcano plot was universally used to illustrate the bonding energy between the active sites and intermediates, which could be split into two legs from the apex representing the strong and weak binding [Figure 4B][89]. The complexes on the ascending segment bind strongly with the *O intermediates and catalyze the reduction of 4e$^-$ ORR, and the release of -OH is the key step determining the final activity. While the complexes on the descending segment (weakly bound side) usually catalyze the 2e$^-$ ORR[90]. Tuning the binding energy to reach the apex of the ORR volcano plot has proved to increase the activity of the M-N-C catalyst effectively.

ORR durability

M-N-C catalysts have revealed huge potential in replacing PGM catalysts for ORR with respect to the initial activity, but the Achilles' heel remained in their poor stability under an acid medium. Therefore, the universal procedures to research catalyst durability are necessary for settling the key problem. Carbon

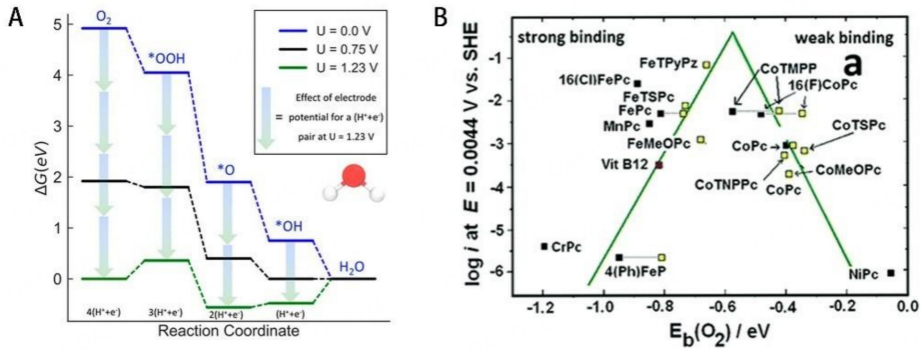

Figure 4. (A) Free energy diagram of 4e⁻ ORR on Pt. This figure is quoted with permission from Kulkarni *et al.*[87]. (B) M-O_2 adsorption energy. This figure is quoted with permission from Zagal *et al.*[89].

corrosion, as well as the durability of catalysts, are related to the concentration of H_2O_2 and ROS. The rotating ring-disk electrode test was widely used to measure the yield of H_2O_2. However, the generation of ROS by the Fenton reaction between Fe^{3+} and H_2O_2 leads to severe degradation of catalyst performance and is also a major factor in the degradation of PEM. The Fenton reaction is shown as follows:

$$Fe^{2+} + H_2O_2 + H^+ \rightarrow Fe^{3+} + H_2O + OH^* \quad (23)$$

So, the content of ROS is a more significant parameter for evaluating the durability of catalysts because ROS can oxidize and destroy catalysts easily. Chen *et al.* used 7-hydroxyl coumarin as the probe to detect the content of OH* by analyzing the fluorescence intensity [Figure 5A][91]. Similarly, Xie *et al.* carried out the 6-carboxy fluorescein (6-CFL) dye as a fluorescent molecular and detected the content of ROS by comparing the fluorescence decay[78]. Moreover, 5,5-dimethyl-1-pyrroline-*N*-oxide (DMPO) was used as a spin trap for OH* to prolong the lifetime of OH* so electron paramagnetic resonance (EPR) could detect the content of ROS. Our group proposed an *in situ* experiment to detect the content of ROS[25]. The mechanism is that ABTS (2, 20-azinobis (3-ethylbenzthiazoline-6-sulfonate) could react with ROS and convert to ox-ABTS which induced the color change documented by UV-vis absorption spectra [Figure 5B]. The Cr-N-C catalyst shows a much smaller change than that of the Fe-N-C system, so the stability is higher. Theoretical calculations can also be used to predict catalyst durability. Xie *et al.* used theoretical calculations to predict the adsorption ability of different sites for ROS and H_2O_2 [Figure 5C][78]. The adsorption energies of ROS and H_2O_2 on Fe-N-C were higher than TaO_2-OH, indicating that the TaO_2-OH moieties trended to be attacked by ROS and thereby protecting Fe-N-C sites.

KEY STABILITY ISSUES OF M-N-C CATALYSTS

Carbon corrosion

Carbon corrosion can be primarily divided into chemical corrosion and electrochemical corrosion. These two typical types of carbon corrosion generally involve oxidation and structural damage of the carbon matrix, which are the primary degradation mechanisms of M-N-C catalysts. In general, electrochemical corrosion is always ignored because it only happens at high potential (E > 0.9 V) and the sluggish kinetic also hinders the occurrence[92]. However, in the fuel test, severe electrochemical corrosion will happen in the following situation. The absence of H_2 and the presence of O_2 in start-up and shut-down states result in a cathode transient potential of around 1.4 V[93]. Fuel starvation can cause a high anode potential of up to 1.6 V. The addition of oxygen evolution reaction (OER) catalysts on the electrode surface may be a feasible way to reduce the electrochemical corrosion of carbon matrix[94]. Severe carbon corrosion would lead to the

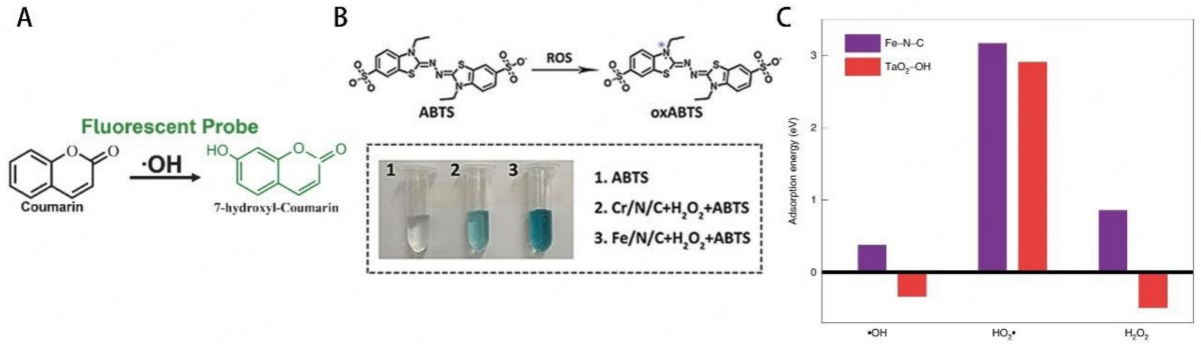

Figure 5. (A) Schematic illustration of the conversion of non-fluorescent coumarins to fluorescent 7-hydroxycoumarins by OH*. This figure is quoted with permission from Chen *et al.*[91]. (B) The reaction between ROS and ABTS, and the color change of the solution after the Fenton reaction. This figure is quoted with permission from Luo *et al.*[25]. (C) The adsorption energy of H_2O_2 and ROS on the surface of Fe-N-C and TaO_2-OH. This figure is quoted with permission from Xie *et al.*[78].

collapse of the carbon matrix and falling/aggregation of active sites, which will enormously impact the activity and stability of the catalysts. Carbon corrosion could also drive the demetallation of MN_4 sites next to oxidized carbon atoms, increase the mass-transport resistance around the remaining active sites, reduce the active site density and electron conductivity, and reduce the electrode porosity[28]. Therefore, carbon corrosion was regarded as the main cause of activity loss. As shown in Figure 6A, the attack of ROS eventually induced the degradation of the active sites and the formation of FeO_x particles. However, another kind of mild oxidation at the carbon surface reduced the TOF of FeC_xN_y moieties by increasing the binding energy with O_2[95]. This kind of mild oxidation was restricted to the top surface without the formation of volatile CO or CO_2. In conclusion, the attack of ROS induces carbon oxidation decomposition active centers, and the leached iron ions, in turn, promote the formation of ROS from H_2O_2 through the Fenton reaction.

Demetallation

The demetallation of active sites is the direct cause of activity decay during ORR. Distinguishing M-N_x/C active sites in metal/metal compounds and identifying which kind of mental leaching will directly lead to the loss of activity is the prerequisite for elucidating the demetallation mechanism during long-term ORR. Most of the Fe leaching during the ORR process originates from inactive and acid-soluble iron species such as Fe nanoparticles/oxides/sulfides/carbides[96].

Choi *et al.* applied a scanning flow cell connected to an inductively coupled plasma mass spectrometer (SFC/ICP-MS) to reveal the demetallation mechanism[97]. They synthesized three kinds of Fe-N-C catalysts. The first Fe-N-C catalysts included a mass of both FeN_xC_y active moieties and Fe particles as a reference (denoted as FeNC-wet-1). The second Fe-N-C catalysts had low amounts of Fe particles and a mass of FeN_xC_y active moieties (denoted as FeNC-dry-1). The third Fe-N-C catalysts contained FeN_xC_y active moieties and undetectable Fe particles [Figure 6B]. These different Fe particle contents in Fe-N-C catalysts were then analyzed using EXAFS and Mössbauer spectroscopy. For FeNC-wet-1 catalysts, Fe leaching could be observed evidently in the initial 20 fast cyclic voltammograms (CVs) (ca. 705 $\mu g_{Fe} g_{cata}^{-1} l^{-1}$). However, the Fe leaching amount of FeNC-dry-1and FeNC-dry-0.5 was less, ca. 87$\mu g_{Fe} g_{cata}^{-1} l^{-1}$and no more than ca.10 $\mu g_{Fe} g_{cata}^{-1} l^{-1}$, respectively. Although there was a huge discrepancy in the amount of Fe precipitated in the different catalysts. Surprisingly, they had similar tendencies in fuel cell tests in the first 50 h. They both exhibited high initial ORR activity and decreased slowly during the fuel cell testing. Therefore, the leaching of Fe from Fe particles could not lead to the loss of initial activity, but the leached iron ions would catalyze the Fenton

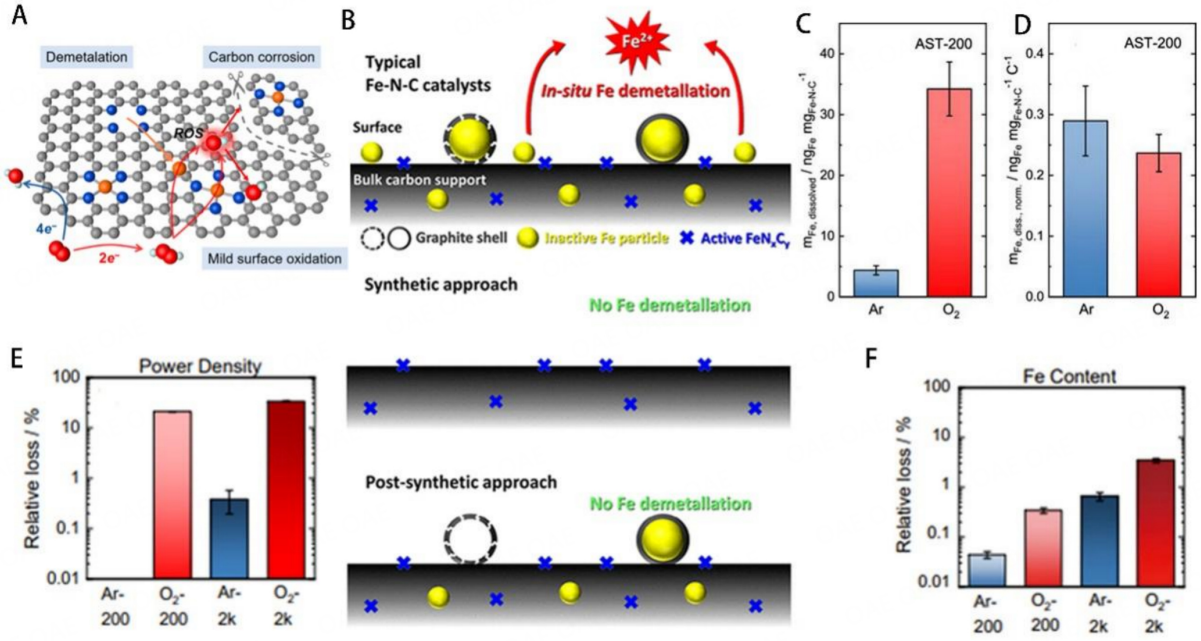

Figure 6. (A) Schematic illustration of the carbon corrosion mechanisms. This figure is quoted with permission from Wan *et al.*[99]. (B) Schematic demonstration of three models of Fe-N-C catalysts composed of Fe particles, Fe particles with a carbon layer, and FeN_x sites. This figure is quoted with permission from Choi *et al.*[97]. (C) Comparison of the quantity of leached metal after 200 cycles AST (O_2 or Ar environment) in alkaline media. (D) The amount of dissolved Fe normalized to the applied electric charge. Relative losses of the power density (PD) at 0.65 V RHE (E) and the Fe content (F) over the Ar-AST-200, O_2-AST-200, O_2-AST-2000, or Ar-AST-2000 procedures. These figures are quoted with permission from Ku *et al.*[98].

reaction, which further promoted the formation of ROS and reduced the activity of the catalysts.

To elucidate the mechanism of demetallation, Xie *et al.* applied DFT calculation to predict the demetallation process of MN_4 sites[22]. The proposed metal leaching mechanism is that the metal center of MN_4 sites moves away from the state coordinating with N_4 to the carbon surface and combines with two N atoms, the other two N atoms bond with H in acid media. Then the Fe center adsorbed O_2 moves away from the plane and further leaches off the active sites.

Recently, Ku *et al.* proposed that different gas environments might induce different rates of demetallation of active sites in alkaline media[98]. By comparing the content of iron leaching in the different environments (O_2, Ar), more iron leaching in the O_2 environment than in the Ar environment was observed after 200 cycles AST [Figure 6C]. The linear relationship between the leaching rate of Fe and the number of electric charges indicated the correlation of current density with Fe dissolution at relatively high current densities [Figure 6D]. On the contrary, no correlation was observed between Fe dissolution and the number of potential cycles. Furthermore, the relation between the Fe leaching rate and the power density change was further discussed. Around 3.4% loss of Fe content after O_2-AST-2000 induced the 34% loss of power density [Figure 6E and F]. This prominent power density in the O_2 environment loss could not be fully attributed to the demetallation of FeN_4 moieties, which might be related to the Fe leaching of the inactive site. An apparent decrease of the C-C signal in XPS C 1s proved that the carbon shells of Fe_3C were destroyed, exposing the Fe_3C moieties, which further induced the Fe leaching of Fe_3C and the decrease of TOF. Fe_3C might participate in the ORR process, as Jiang *et al.* reported[39]. The Fe_3C nanoparticles might facilitate the adsorption of oxygen molecules. Thus, the coexistence of high content of FeN_4 and sufficient metallic iron nanoparticles was essential for the high ORR activity. Furthermore, the S-number (the reciprocal of the

charge-normalized dissolution) was used to account for charge-normalized dissolution. During the first 1500 cycles AST, the S-number stabilizes around 10^{-6} (around 10^{6} electrons transfer for a leached Fe atom). The S-number increased significantly after 1500 cycles, which was consistent with the rapid decay of the initial catalytic performance and subsequent stabilization. In previous reports, the demetallation of the catalysts was widely recognized as the primary factor contributing to catalyst instability issues. The demetallation of active sites will directly induce the degradation of catalytic performance. The demetallation of inactive Fe particles will also lead to the decrease of TOF and enhanced Fenton reaction. Therefore, improving the intrinsic demetallation resistance of active sites is an effective way to improve catalyst stability.

Nitrogen protonation

The nitrogen protonation process is the N atoms of MN_4 moieties combine with H to form N-H bonds, which is considered to be the rate-determining step in the degradation of the MN_4 moieties[46]. After nitrogen protonation, the M-N bonds tend to break and the metal center will move away from the N_4 plane and leach out during ORR. The protonation process involves attaching one or two hydrogen atoms to the surface of active moiety. Nitrogen protonation affected the C-N bond stability of the pyridinic-N doped graphene (PNG) and oxidized PNG (PNG-O). After protonation, the Fe-N bond would considerably stretch[100]. PNG and PNG-O exhibited different degrees of Fe-N bond elongation after nitrogen protonation, indicating that the adsorption of O_2 could promote the stretching of the Fe-N bond. Moreover, OH* could also promote the stretching of Fe-N bonds and demetallation of active sites; if two OH* bound to the metal site on the same side, the Fe centers would form the fragile $*M(OH)_2$ oxidation intermediates[101]. The $*M(OH)_2$ intermediates were susceptible to successive N protonation that eventually caused irreversible damage to active sites [Figure 7]. The nitrogen protonation process further induced the demetallation and reduction of catalytic activity. Herranz *et al.* especially investigated N-protonation and anion-binding effects on Fe-N-C catalysts[102]. They concluded with two hypotheses. The FeN_4 sites had high TOF when the active center was near the unprotonated N-groups and bound to the anions during ORR. Once the basic N-groups were protonated, the TOF of the FeN_4 site would be extremely decreased. The pace of the step is dependent on the speed of polymeric chains in reaching the N-groups. In this hypothesis, the protonation of pyridinic nitrogen might be the main reason for the activity decay of PGM-free catalysts. Another hypothesis was that the FeN_4 site kept high TOF when the near N-groups were protonated without anion bonds. However, the TOF of FeN_4 site will decrease when the anion bond with FeN_4 center. In this case, protons can rapidly access the basic N-groups, but the anions will not immediately follow with the protons. This hypothesis could be used to explain the catalytic performance of M-N-C catalysts, which exhibited high initial activity followed by a rapid decrease. In general, the nitrogen protonation process is the main reason for the decrease of TOF and the key step in the demetallation of the MN_4 sites.

Water flooding

M-N-C catalysts with excellent performance often possess many micropores on the carbon basis in which most active sites are embedded. When the water is trapped by the micropores, the formation of three-phase interfaces is hindered and the diffusion of O_2 to the active sites is difficult. This undesired process is called water flooding.

Li *et al.* have shown that severe water flooding occurred in thick electrode layers, which might be the main cause of the initial activity loss in the MEAs[103]. Due to the hydrophilicity of the porous carbon matrix and the chemisorption capacity of the catalyst, the micropores of the M-N-C catalyst tended to be blocked. The blocked micropores would further hinder access to oxygen and the loss of activity sites in the micropores[104]. However, Choi *et al.* proposed the opposite view for microporous flooding[105]. They compared the degree of micropore flooding with the observed activity loss in MEA tests. During the *in situ*

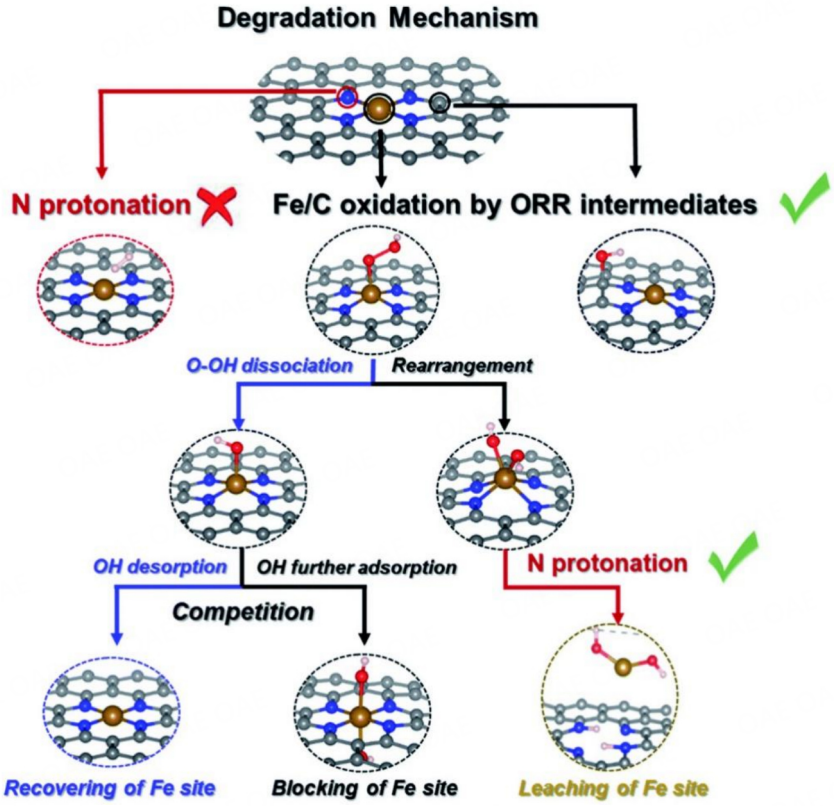

Figure 7. Mechanism of the demetallation induced by N protonation. This figure is quoted with permission from Yang *et al.*[101].

stability test, this negligible submerged micropore was unlikely to be the main reason for performance degradation. Hence, the mechanism of micropores flooding is still unclear and needs further research.

STRATEGY FOR DURABILITY IMPROVEMENT

Stable carbon matrix

Previous studies have demonstrated that highly graphitized catalysts could significantly improve the stability of catalysts[106]. The highly graphitized carbon substrate can enhance the hydrophobicity of the catalyst, protect the catalyst from severe micropore flooding, improve the active site stability, and further improve the demetallation and corrosion resistance of the catalyst[107]. Therefore, designing a more graphitized local structure of catalysts is a feasible way to improve catalyst stability. Higher pyrolysis temperature could induce higher a degree of carbon-based graphitization[17]. Qu *et al.* designed Fe-N_x/C catalysts via a stepwise pyrolysis treatment which achieved a highly graphitized carbon and superior stability[108]. Only 25 mV loss of half-wave potential after 30000 cycles ADT and high retention rate of activity after 100 h fuel cell test proved the role of high levels of graphitized carbon substrates in enhancing catalyst stability. Similarly, Yan *et al.* designed a nitrogen-doped bimetallic carbide-graphite catalyst achieving ultra-high stability in alkaline media[77]. The catalyst (noted as N-Fe_2MoC-GC) was synthesized at high temperatures (1300-1400 °C), which achieved a high degree of graphitization of carbon matrix. After the durability test, no apparently increasing in particle size in N-Fe_2MoC-GC was observed. Therefore, high degree graphitization of carbon matrix could exceedingly improve the stability of catalysts. Recently, Li *et al.* synthesized ordered and interconnected macropores of carbon matrix [Figure 8A and Figure 8B] with FeCo alloy nanoparticles[74]. The interconnected microporous and hierarchical porous carbon matrix provided channels for mass transfer and exceedingly facilitated the exposure of active sites. The relationship between

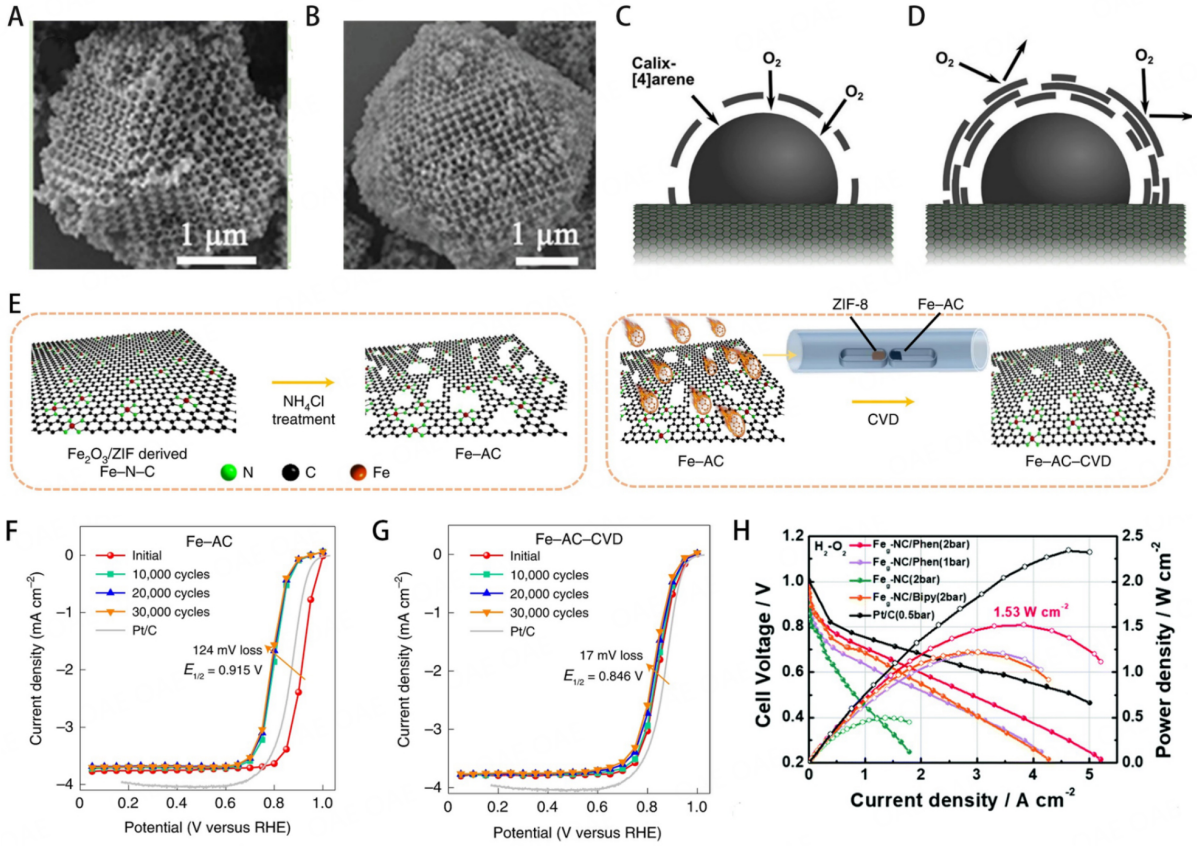

Figure 8. (A, B) Field-emission scanning electron microscopy (FESEM) image of 3D ordered porous ZIF-67 taken from different directions. These figures are quoted with permission from Li *et al.*[74]. Thin (C) and thick (D) carbon shell models. These figures are quoted with permission from Yoo *et al.*[109]. (E) Schematic demonstration of Fe-N-C catalyst with NH_4Cl treatment and deposit of a carbon layer on the Fe-AC catalyst. (F, G) ORR polarization curves after different cycles AST text in O_2-saturated 0.5 H_2SO_4. These figures are quoted with permission from Liu *et al.*[46] (H) H_2-O_2 PEMFCs polarization and power density curves. Cathode, 3.5 mg_{cat} cm^{-2} for Fe-N-C; anode, 0.4 mg_{Pt} cm^{-2}. This figure is quoted with permission from Yin *et al.*[81].

Fe and Co was elucidated by DFT calculation, and the catalysts achieved a lower energy barrier for the adsorption of intermediates. The introduction of Fe into Co induced the d-band center of Co closer to the Fermi level, which accelerated the adsorption of intermediates. Furthermore, the high stability of the catalyst was mainly due to the strong interaction of FeCo alloy nanoparticles and porous carbon matrix, and only a small amount of metal leaching was measured after the stability test. The high durability performance and minimal metal leaching of the catalysts manifested that the activity sites were firmly anchored on the ordered porous carbon matrix.

The carbon layer could effectively improve the durability of catalysts by preventing the catalysts from being attacked by ROS. Yoo *et al.* summarized the strategy of designing carbon shells on catalyst surfaces and discussed the relationship between the structure of carbon shells and the durability of catalysts[109]. On the one hand, the carbon shell provided a physical parclose that could protect the catalysts from ROS and H_2O_2 attack. On the other hand, the carbon shell maintained active sites and prevented metal sites from agglomeration during the ORR, thus keeping high accessible surface area. The thickness of the carbon shell was a significant influencing parameter for catalytic performance, and a thin carbon shell (< 1 nm) allowed the permeation of reactants during the ORR [Figure 8C]. However, a thick carbon shell (> 3 nm) had redundant coverage of active sites, which would hinder mass transport [Figure 8D]. Liu *et al.* developed a

novel strategy to synthesize a more stable Fe-N-C catalyst via chemical vapor deposition (CVD), depositing an N-doped carbon layer on the Fe–N–C catalyst, resulting in excellent stability[73]. Gaseous deposition of 2-methylimidazole on Fe-doped ZnO substrates followed by thermal activation at 1000 °C to from the thin carbon layer (< 1 nm). Recently, Liu *et al.* reported a method for chemical vapor deposition of ZIF-8 onto Fe-AC[46]. As shown in Figure 8E, NH_4Cl treatment could create amounts of defects in the carbon matrix. Further, the CVD method was used to improve the durability of the Fe-AC catalyst. On the one hand, the deposited C-N source on the catalyst could form a thin carbon layer that physically protects the active site from ROS attack. On the other hand, the CVD process could promote the transfer of S1 sites to S2 sites. As shown in Figure 8F, the Fe-AC exhibited the best ORR activity in RDE test with a half-wave potential of 0.915 V. Unfortunately, such high ORR activity decreased strikingly ($E_{1/2}$: 0.915 V-0.791 V) after 30000 cycles AST test. Therefore, the CVD technique was used to solve the unstable issue. With a decrease in ORR activity, the stability of Fe-AD-CVD was increased considerably [Figure 8G]. Achieving both high activity and high durability in one catalyst remains difficult, and it is important to unravel the degradation mechanisms. The CVD technique can be used not only to deposit C-N sources to improve catalyst stability but also to deposit metal sources. Sun's group report a CVD method that deposits $FeCl_2$ on a surface-rich pyridinic-N carbon matrix, achieving a high density and accessibility of FeN_4 sites[81]. The ORR activity of Fe_g-NC/Phen in PEMFC even reached the DOE (2025) target with a current density of 46 mA cm^{-2}@0.9 V and a P_{max} of 1.53 Wcm^{-2}(H_2-O_2), which is almost the best reported performance of M-N-C catalysts in MEA [Figure 8H]. The performance of MEAs is not only related to the ORR capability of the catalyst but also related to the MEA preparation process, catalyst ink, and test conditions. Seizing gaseous Fe^{2+} on the carbon matrix increased the density of surface FeN_4 sites with high utilization. The introduction of defects in the carbon matrix can also improve the accessibility of the active substance. Kim *et al.* embedded FeCo alloy nanoparticles into a defect-rich N-doped carbon matrix[110]. The carbon matrix was oxidized by the appropriate amount of H_2O_2. A great number of defect sites and a high surface area carbon matrix in the catalyst improved the accessibility of active sites. The encapsulated alloy nanoparticles were protected by the carbon layer that prevented corrosion and aggregation, achieving high stability during the ORR. Therefore, regulating the structure of carbon support is essential to improve catalytic performance. The carbon matrix could not only anchor the active site on the carbon matrix but also change the electronic structure of the metal centers, which was related to the intrinsic activity of the catalysts. Therefore, designing the carbon matrix is a feasible method to improve the performance of catalysts.

Regulation of the M-N_x bonds

The length of the Fe-N bond is an essential parameter affecting the stability of catalysts. Building robust Fe-N bonds can reduce the prolongation caused by absorption of oxygenated intermediates, further increasing the resistance of demetallation. In a recent study by Ohyama *et al.*, *in situ* XAS was used to analyze the durability of the 14-mcembered hexaaza macrocyclic Fe complex (Fe-14MR) [Figure 9A] and Fe phthalocyanine (FePc) [Figure 9B][111]. As shown in Figure 9C and Figure 9D, the CV peak of Fe-14MR/C was weakened to a lower degree than FePc, indicating that Fe-14MR/C was more resistant to demetallation than FePc during ORR. Furthermore, the Fe concentrations of catalysts were monitored by Fe-derived X-ray fluorescence. The Fe leaching rate of 14-membered ring ligands was much lower than FePc in acid, which also indicated the higher durability of the catalysts [Figure 9E]. Therefore, regulating the length of Fe-N bonds was key to the stability of the Fe-14MR during the ORR. It was the shorter Fe-N bond and more compact ligands that led to the high stability of Fe-14MR. Changing the binding constant and chelation of the metal center was a feasible way to regulate Fe-N bond length and further reduced the demetallation of FeN_4 active sites. Increased temperature also resulted in shorter Fe-N bonds[112]. Miao *et al.* successfully synthesized P(AA-MA) Fe-N catalysts and regulated the lengths of Fe-N bonds by manipulating the rate of acrylic acid and maleic acid during the copolymerizing process[67]. PAA-Fe-N catalyst was used as a reference and was synthesized from homopolymerization of acrylic acid and other precursors with shorter

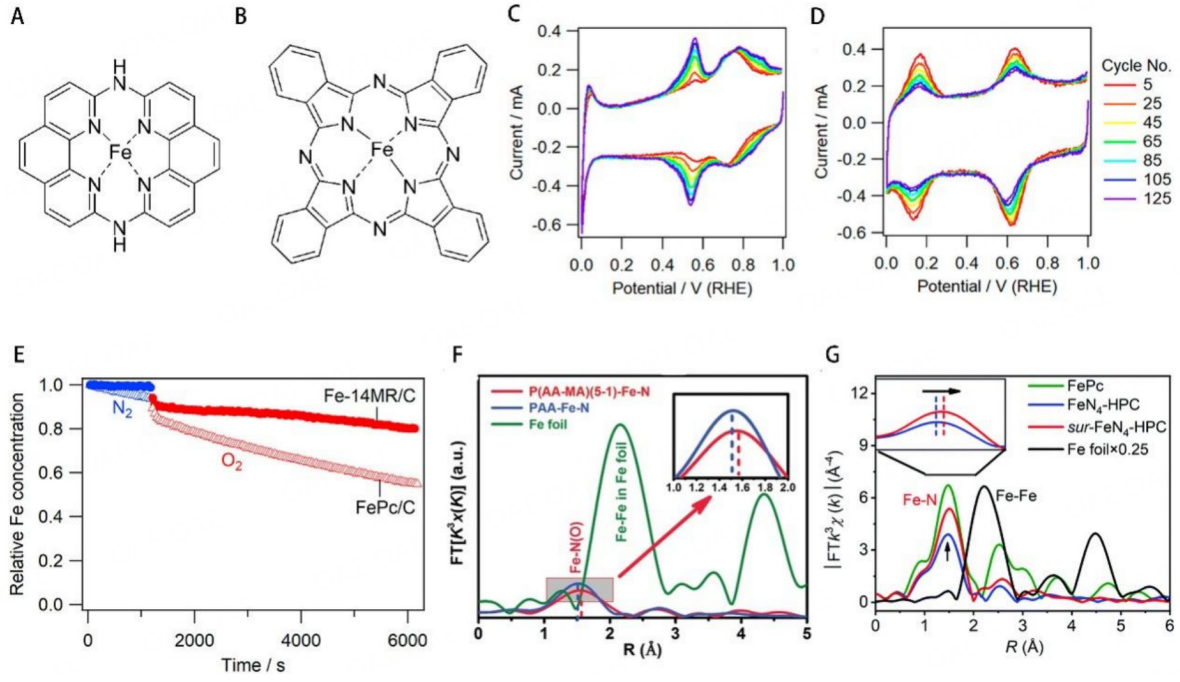

Figure 9. Schematic demonstration of the structure of Fe14MR (A) and FePc (B). CV curves for Fe-14MR/C (C) and FePc(D). (E) Relative concentration changing of Fe in Fe-14MR/C and FePc during CV cycling under N_2 and O_2. These figures are quoted with permission from Ohyama *et al.*[111]. (F) k^3 -weighted FT-EXAFS spectra of P(AA-MA)(5-1)-Fe-N, PAA-Fe-N, and Fe foil samples. This figure is quoted with permission from Miao *et al.*[67]. (G) k^3 -weighted FT-EXAFS spectra of sur-FeN_4-HPC, FeN_4-HPC, FePc, and Fe foil. This figure is quoted with permission from Chen *et al.*[68].

Fe-N bonds. Fe-N bonds of different lengths for the P(AA-MA)Fe-N and PAA Fe-N catalysts were verified by XAS [Figure 9F] and Mössbauer spectroscopy. Moreover, isothermal titration calorimetry (ITC) was applied to measure the binding constant stoichiometry of ligands and metal ions. The binding constant of Fe^{3+} to P(AA-MA) was higher than Fe^{3+} with PAA or MA. As expected, the P(AA-MA) Fe-N catalysts had higher stability and activity than PAA Fe-N catalysts during the durability test. A similar consequence was achieved by Chen *et al.*[68]. Hierarchically porous N-doped catalysts were synthesized by pyrolysis followed by HF etching to remove Zn and SiO_2 from the substrate (note as surf-FeN_4-HPC). The catalysts achieved high accessibility of active sites by anchoring abundant FeN_4 sites at the carbon edges. As shown in EXAFS spectra [Figure 9G], surf-FeN_4-HPC had a longer length of Fe-N bonds than FeN_4-HPC (anchoring on basal-plane) and achieved high durability, with only 20 mV loss of half-wave potential after 20000 cyclic voltammetry scans. These two above consequences seemed to conflict with other studies. Li *et al.* synthesized Fe-pyridinic N-C catalysts with a higher ratio of pyridinic N than Fe-N-C catalysts[69]. Fe-pyridinic N-C catalysts achieved both better activity and stability than Fe-N-C catalysts. DFT calculation showed that pyridine-type FeN_4 had a higher Gibbs free energy during the Fe leaching process. The bond lengths of Fe-N to pyridine nitrogen and pyrrolic nitrogen were 1.88 and 2.08 Å, respectively, which also supported that the shorter Fe-N bond was stable. A similar consequence could also observe in CoN_4 sites, and the Co-N-C catalysts exhibited outstanding resistance to metal leaching, which might be related to the shorter Co-N bond length[22]. The Co-N bond of Co-N-C (1.94 Å) was shorter and more stable than porphyrin-like CoN_4C_{12} (2.01 Å)[72].

In a recent study by Wan *et al.*, the introduction of Fe clusters near FeN_4 sites with two-dimensional porous carbon (noted as Fe_{SA}/Fe_{AC}-2DNPC) achieved excellent catalytic performance during the ORR[72]. The strong interaction of Fe clusters and FeN_4 sites could change the electronic structure of active sites and lead to a

much more suitable absorption strength of ORR intermediates [Figure 10A]. The schematic of ORR is shown in Figure 10B. Fe_{SA}/Fe_{AC}-2DNPC lost only 18 mV of half-wave potential after 10,000 potential cycles in an O_2-purged acidic medium. Then DFT calculation was used to elucidate the possible mechanism; the interaction between the Fe cluster and FeN_4 promoted the axial adsorption of OH at the Fe center while the other side of FeN_4 was used for ORR. $Fe(OH)N_4$ achieved a lower limiting energy barrier and enhanced ORR activity. Several models were built to elucidate the catalytic performance of FeN_4 sites near different Fe clusters (Fe_4-N_6, Fe_{13}-N_6, Fe_4-C_6). The different numbers of Fe atoms in the cluster have no obvious effect on the activity enhancement; on the contrary, the effect of N-coordinated Fe clusters on FeN_4 centers is greater than that of C-coordinated Fe clusters. Furthermore, molecular dynamic simulation was carried out to obtain the Fe-N radial distribution function, which could be used to illustrate the Fe-N bond length [Figure 10C]. The average Fe-N bond lengths in FeN_4 were 1.82-2.38 Å, which were slightly longer than that of Fe-N_4/Fe_4-N_6 (1.82-2.22 Å), indicating that FeN_4 sites near Fe_4-N_6 clusters are more stable than bare FeN_4 sites. The Fe-N bond lengths of bare FeN_4 sites were considerably stretched from 1.82-2.38 Å to 1.71-2.50 Å; on the contrary, Fe-N_4/Fe_4-N_6 still kept compact distribution, and short Fe-N bond lengths of 1.86-2.06 Å, which correlated with the high stability of Fe_{SA}/Fe_{AC}-2DNPC, even at the elevated temperature. The compact distribution of Fe-N bonds might be attributed to the incoherent vibrations of Fe clusters and single Fe atoms. The Fe_4-N_6 clusters increased the stability of the active center by building robust Fe-N bonds. However, the Fe^{3+} from the Fe clusters seemed to contradict the mitigates of the Fenton reactions to minimize ROS generation. Notably, the Fe_{SA}/Fe_{AC}-2DNPC demonstrated higher stability relative to references, which included the catalysts containing only bare FeN_4 sites (Fe_{SA}-2DNPC) and the catalysts containing Fe nanoparticles and FeN_4 sites (Fe_{SA}/Fe_{NP}-2DNPC). The atomic Fe clusters were chemically bound to the carbon matrix and kept stable in acid media[113]. Some researchers reported that the metal cluster or nanoparticle in Fe-N-C catalysts improved the ORR activity in both RDE and MEA testing[114,115]. However, the unstable Fe cluster would be leaching and transferred ions, which promoted the Fenton reaction and reduced the conductivity of Nafion under the test condition[116]. Thus, the regulation M-N_x bonds by introducing metal clusters and nanoparticles should be cautious due to the degradation mechanism in PEMFCs.

Introduction of the fifth ligand

The demetallation of active centers may involve the adsorption of ORR intermediates in the axial direction of metal center. The introduction of the fifth ligand can reduce the elongation of M-N bond. Recent studies have shown that Fe centers could spontaneously adsorb ORR intermediates to adjust the electronic structure of the FeN_4 active sites and catalyze ORR with O_2 at another side[117]. Their calculation found that the Fe centers of Fe-N-C catalysts tend to be covered with OH* in wide potential rage (0.28-1.00 V) and the adsorption energy optimized by the OH* intermediates so that these sites achieved enhanced ORR performance [Figure 11A]. The theoretical result indicated that $Fe(OH)N_4$ structure exhibited higher half-wave potential (0.88 V) and was closer to the actual result than bare FeN_4 in catalyst [Figure 11B]. Our group concluded that RuN_4OH structure was the actual active site in the Ru-N-C catalysts[118]. As shown in Figure 11C, RuN_4OH structure achieved downhill in free energy for each step at U=0 V due to the presence of the -OH, which demonstrated facile reaction progress for ORR. The introduction of -OH downshifted the d-band center of Ru and reduced the adsorption energy for *OH intermediates. As shown in Figure 11D and Figure 11E, the linear relationship between the adsorption energy, overpotential, and Bader charge of Metals proved that the -OH ligand changed the electronic structure of the metal center, so the Ru-N-C catalysts move close to the volcano apex and achieve the high ORR performance.

The MN_4 site tends to be covered by molecules in the axial direction, forming a 5-coordinated or 6-coordinated structure, but these weak ligands may not keep stable in working conditions. *In situ* Mössbauer spectroscopy and XAS can be used to detect adsorbed species on FeN_4 surfaces. Unfortunately, the time

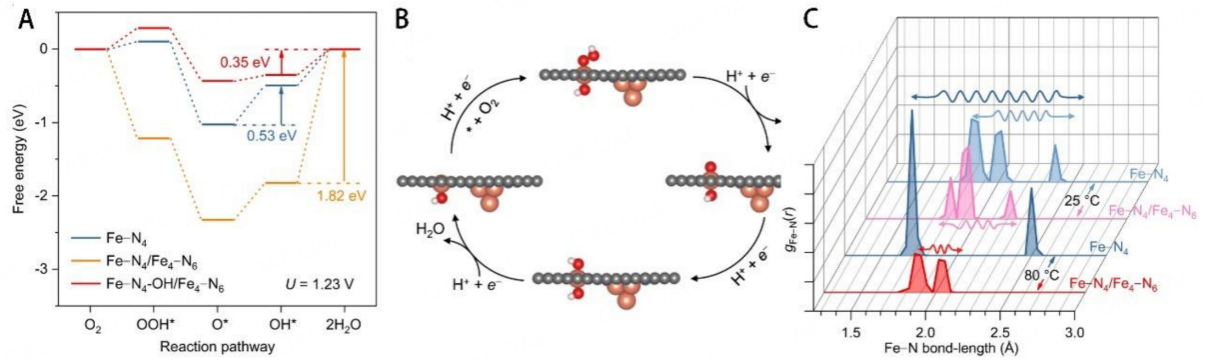

Figure 10. (A) Free energy diagrams at 1.23 V for ORR over three types of active sites of Fe-N_4, Fe-N_4/Fe_4-N_6, and Fe-N_4-OH/Fe_4-N_6. (B) Schematic ORR process on the Fe-N_4 site of Fe-N_4/Fe_4-N_6. (C) Fe-N radical distribution function of the Fe-N_4 site in the models of Fe-N_4 near Fe_4N_6 and bare Fe-N_4 site at 25 °C and 80 °C. These figures are quoted with permission from Wan *et al.*[72].

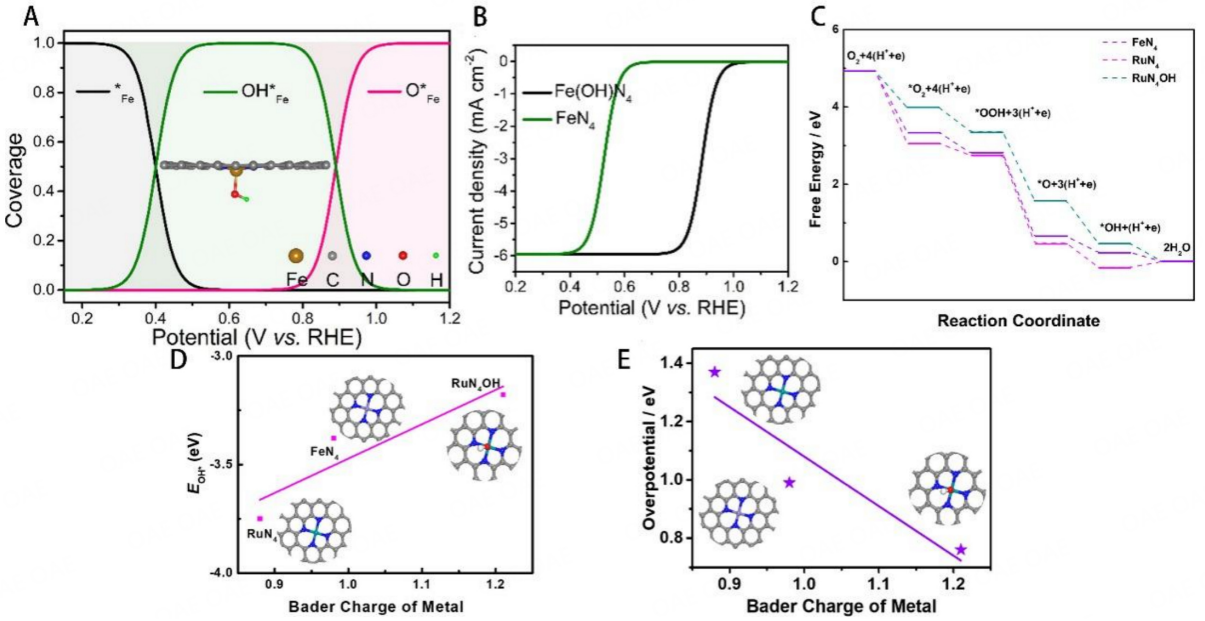

Figure 11. (A) Coverages of the ORR intermediates on the Fe center as a function of U. (B) Simulated ORR polarization curves of Fe-N-C catalysts based on FeN_4 and $Fe(OH)N_4$ centers. These figures are quoted with permission from Wang *et al.*[117]. (C) Gibbs free energy diagram for ORR. (D) Linear relation between Bader charge of the mental and binding energy of ORR intermediates. (E) Linear relation between Bader charge of mental and overpotential. These figures are quoted with permission from Xiao *et al.*[118].

resolution is not enough to monitor the fast changes of adsorbed species on the surface of the active sites, which hinders the cognition of the relationship with axial coordination and performance. Therefore, it is necessary to develop in-situ and operando characterization techniques to resolve the dynamic mechanism and design effective electrocatalysts.

To elucidate the influence of ORR intermediates on the durability of FeN_4 centers, Wei *et al.* used *in situ* spectroscopy to illustrate the interaction between FeN_4 active sites and ORR intermediates[119]. During the ORR process, Fe centers would move away or toward the plane when the FeN_4 site adsorbs the ORR intermediates. As shown in Figure 12A, the 593 cm^{-1} Raman band was attributed to the vibration of in-plane Fe-N_4[120]. Notably, in acid media, the Raman band at 593 cm^{-1} attenuated considerably at a lower potential

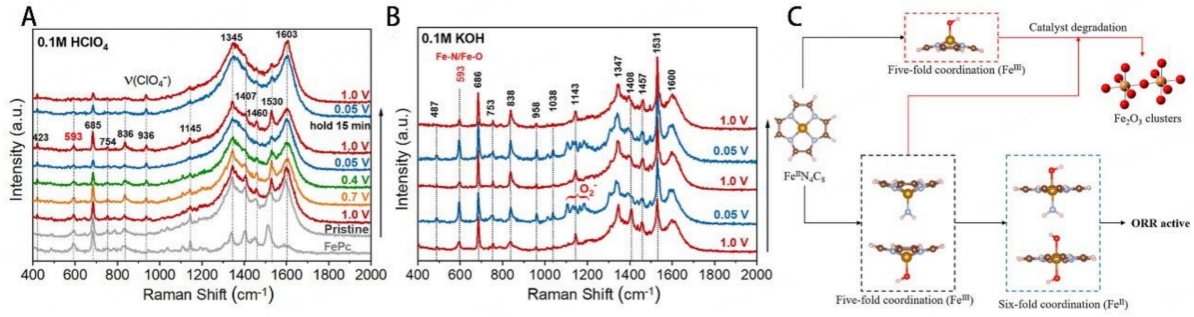

Figure 12. *In situ* Raman spectroscopy of FePc/C during ORR in (A) acid solution and (B) alkaline solution. These figures are quoted with permission from Wei *et al.*[119]. (C) ORR mechanism at fourfold coordination FeN_4C_8 and fivefold coordination FeN_4C_8. This figure is quoted with permission from Nematollahi *et al.*[121].

compared with the spectroscopy at 1.0 V, implying that the Fe centers tend to move away from the plane at a relatively lower potential. This change was reversible when the potential was kept low for a short time and quickly switched back to high potential. Conversely, this change could also become irreversible when the catalyst is kept at a low potential for a long time (~10 min) in acid media. The discrepancy in alkaline media [Figure 12B] was also observed; the enhanced intensity at 593 cm^{-1} with a wide potential range matched with the higher stability of FePc/C catalysts in alkaline media than in acid media. The possible mechanism was that the axial of the FeN_4 site would spontaneously adsorb a hydroxyl to form a more catalytical and stable site. The axial OH* of the $Fe(OH)N_4$ site would desorb at low potential (< 0.5 V) in acid media, while $Fe(OH)N_4$ remained stable over a wide range of potentials in alkaline media[40].

Recently, Nematollahi *et al.* reported the effect of the fifth ligand including -NH_2, -OH, and -SO_4 on the stability of FeN_4 site[121]. In the presence of the fifth ligand, the degree of Fe-N bond elongation during ORR was significantly reduced. The fifth ligand of the Fe center might improve the resistance of demetallation. The possible mechanism was that the fifth axial ligand at the FeN_4 site could pull the Fe center back into the plane rather than being pulled out of the plane by ORR intermediates [Figure 12C].

Introducing radical scavengers

The addition of radical scavengers to catalysts is an active defensive strategy to reduce the content of H_2O_2 and ROS. The free radicals from the Fenton reaction render catalysts and PEM less durable[122]. The chemical degradations of PEMs are mainly caused by free radical attacks. Therefore, reducing the yield of free radicals was the direct way to improve the durability of PEMFCs. Radical scavengers have been used to improve the durability of PEMs. However, few attempts have been made to introduce radical scavengers into catalysts. Cerium oxide nanoparticles have the excellent scavenging capability of radicals and are widely used radical scavengers[123,124]. Wei *et al.* introduced CeO_2 into the Fe-N-C catalyst, which achieved reduced H_2O_2 production[125]. The CeO_2 could catalyze the reduction of H_2O_2.

$$O_2 + 2H^+ + 2e^- \rightarrow H_2O_2 \quad (24)$$

$$2CeO_2 + 2H^+ + 2e^- \rightarrow Ce_2O_3 + H_2O \quad (25)$$

$$Ce_2O_3 + H_2O_2 \rightarrow 2CeO_2 + H_2O \quad (26)$$

The addition of CeO_2 significantly reduced the production of hydrogen peroxide and ROS, which further improved the stability of the catalyst.

Other metal oxides could also be used as radical scavengers. For example, Xie *et al.* reported a novel method to address the issues of carbon corrosion and demetallation, which are caused by ROS and H_2O_2, by introducing Ta-TiO_x to Fe-N-C catalysts [Figure 13A][78], where the Ta-TiO_x was used as a radical scavenger. To determine the radical scavenging ability of Ta-TiO_x, 6-carboxy fluorescein (6CFL) was used as a dye to measure the content of free radicals [Figure 13B]. Fenton reagent/Ta-TiO_x scavengers exhibited the lowest fluorescence decay, demonstrating the powerful scavenging ability of Ta-TiO_x nanoparticles. Moreover, 5,5-dimethyl-1-pyrroline-*N*-oxide (DMPO) was used as a spin trap for OH* to prolong the lifetime of free radicals, so electron paramagnetic resonance (EPR) could be used to further evaluate the scavenging ability. As shown in Figure 13C, the variation in EPR peak intensity of OH-DMPO with or without Ta-TiO_x/KB proved that Ta-TiO_x nanoparticles significantly decreased the content of free radicals. No apparent change of initial activity after the introduction of scavengers showed that the scavengers well matched up with the Fe-N-C catalysts [Figure 13D]. Ta-TiO_x was introduced into Fe-N-C catalysts as a radical scavenger to catalyze the oxidation from H_2O_2 to O_2 and H_2O and scavenge radicals.

Compared with the introduction of radical scavengers to catalysts, previous strategies to improve durability were the passive way to protect active sites from free radical attacks, such as increasing the degree of graphitization of carbon matrix and etc. However, the addition of radical scavenger additives was a proactive approach to eliminating H_2O_2 and free radicals, which further improved the stability of catalysts.

Designing a diatomic catalyst

To address the instability caused by the Fenton reaction, numerous strategies have been proposed over the past few decades, such as changing the Fe metal center to another transition metal and designing diatomic catalysts. Mn-N-C[26], Co-N-C[22,70], Cu-N-C[24,82], and Sn-N-C[83] catalysts have presented higher stability due to these metal centers with weak Fenton reactivity. Thus, designing diatomic catalysts is an effective way to improve stability and activity of catalysts. The interaction between metal and metal always involves d-orbital hybridization, electronic structure change, and charge density change[126]. In particular, the transition metals have highly variable d-orbitals and spatial geometries; thus, the introduction of another transition metal into Fe-N-C catalysts was an efficient way to regulate the electronic structure of active centers. Recently, our group reported a $FeCoN_5$/C catalyst with Fe-Co dual-atom center sites to decrease the Fenton reaction and boost ORR activity by adjusting the electronic structure of the mental site[80]. The formation energy of $FeCoN_5$ (-11.801 eV) was calculated, which was much lower than FeN_4 (-8.48 eV) and CoN_4 (-7.7 eV), implying the spontaneous formation and higher stability of diatomic centers. $FeCoN_5$/C achieved high catalytic activity with a half-wave potential of 0.86 V and only 13 mV loss after 5000 potential cycles. Homonuclear diatomic catalysts were also a part of diatomic catalysts, our group designed Co_2N_5 diatomic activity sites, which exhibited higher ORR activity than CoN_4 sites[71]. Regulating the neighbor atoms of Fe was an effective way to regulate the spin state of the FeN_4 site. For example, He *et al.*, by neighboring Cu atoms with Fe atoms, successfully regulated the spin state of Fe, which achieved a low H_2O_2 yield (1.2%) and enhanced ORR durability[79]. The interaction of different centers can be regulated via changing bond polarity, atomic distance, bonding coordination, etc. The correlated metal atoms can not only directly bind with the metal center in the first coordination shell, but also bond with the mental center via bridging atoms (O, N, S, *etc.*) in the second coordination shell. Indirect coordination exhibits complicated mutual effects and effective electronic structure adjustment. For example, Liu *et al.* built the bridge bond of Fe-O-Ti[127], and the introduction of Ti into the second coordination shell of the Fe center changed the spin state of the Fe center, resulting in enhanced ORR activity. The introduction of bridge bonds of Fe-O-Fe into catalysts also achieved enhanced catalytic activity[128]. Recently, Peng *et al.* reported a novel catalyst with axial coordination with N rather than another metal atom via the bridge of O atoms (noted as FeN_4-O-NCR)[129]. By theoretical calculation, FeN_4-O-NCR sites were thermodynamically more stable than bare FeN_4 sites. From the PDOS, after the FeN_4 site was axial bridging with the O atom, the 3d-band center of the Fe atom

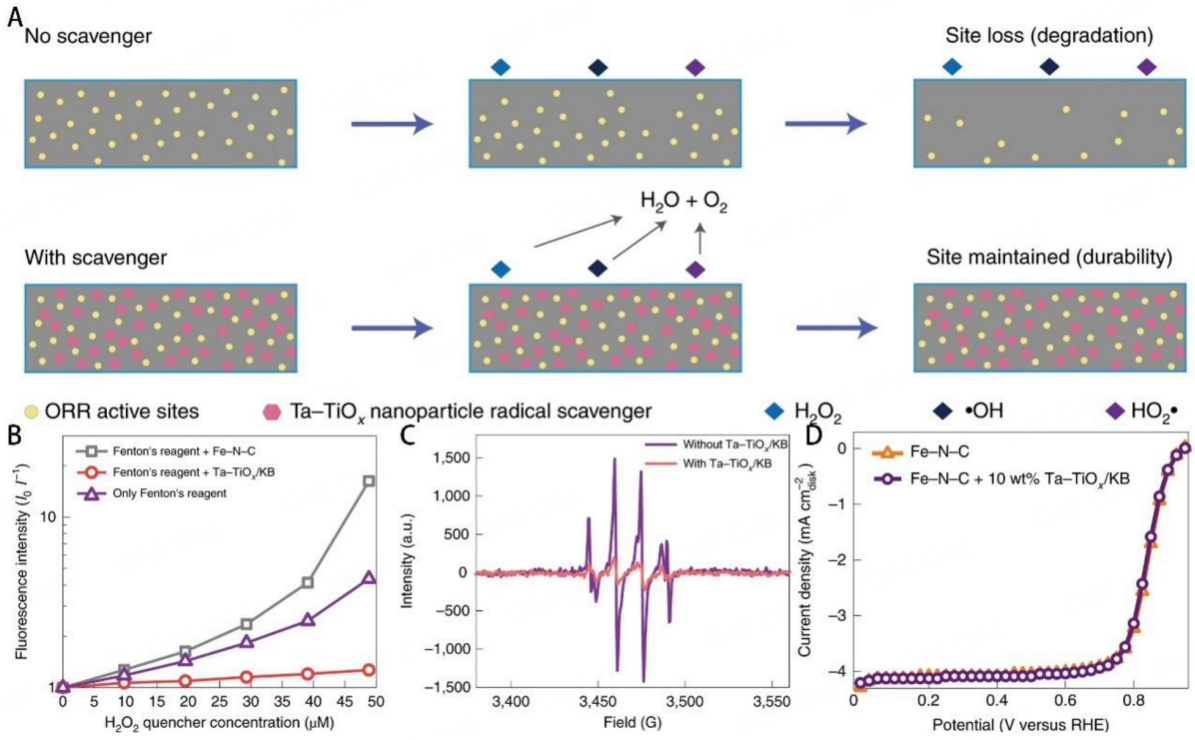

Figure 13. (A) Schematic comparing the PGM-free catalyst in the ORR process without and with the radical scavengers. (B) Stern-Volmer plot obtained using 6CFL dye in the radical solution with Fenton's reagent, Fenton's reagent with Fe-N-C, and Fenton's reagent with Ta-TiO$_x$/KB. (C) Electron paramagnetic resonance spectra of the OH-DMPO. (D) ORR performance of Fe-N-C catalysts with or without the TaTiOx-/KB radical scavengers. These figures are quoted with permission from Xie *et al.*[78].

shifted to a more negative energy direction compared to bare FeN_4 sites [Figure 14A]. Therefore, the appropriate absorption energy of ORR intermediates at active sites and the higher thermodynamically stability led to the enhanced ORR performance of the catalysts. CoN_4 sites exhibited higher resistance to the Fenton reaction and higher stability than FeN_4 sites[22]. Intergrading CoN_4 and FeN_4 into one catalyst may achieve improved stability while maintaining high catalytic activity. Yang *et al.* integrated two single-metal sites, FeNC (shell) and CoNC (core), in the catalysts (noted as p-FeNC@CoNC)[75]. From the result of Raman spectroscopy, p-FeNC@CoNC (0.93) had a medium ratio of I_D/I_G, implying a higher degree of graphitization carbon matrix than p-Fe-N-C (0.84). Therefore, the introduction of the CoN_4 metal center could induce the formation of graphitic carbon matrix. Evidently, the p-FeNC@CoNC catalysts achieved 0.98 V of onset potential and 0.87 V of half-wave potential, only 16mV loss of half-wave potential after 30000 cycles AST in acid media [Figure 14B].

The protonation of active sites is the main reason for the decrease in activity. The active sites trend to combine with H^+, leading to the decrease of TOF in acid media. Recently, Li *et al.* designed a durable half-metallic diatomic catalyst to alleviate the influence of protonation[76]. Six transition metals (M = Mn, Zn, Ni, Cu, Co, Fe) with more than half-filled 3d orbit were selected to separately form bimetal catalyst models with Fe. The free energies (G) of protonation (both one and two hydrogen pathways) were calculated in six bimetal models [Figure 14C and D]. Fe/Zn-N-C catalysts had the highest G of protonation, indicating that the coordination of Fe and Zn atoms achieved excellent resistance to protonation. The Fe/Zn-N-C catalysts showed remarkable durability, exhibiting a half-wave potential of 0.906 V and only 12 mV loss after 5000 potential cycles, which was lower than Fe-N-C (28 mV). Both adsorptions of O_2 and H^+ led to the elongation of M-N bonds, with only a slight change of Fe-N bonds compared with Zn-N bonds. However,

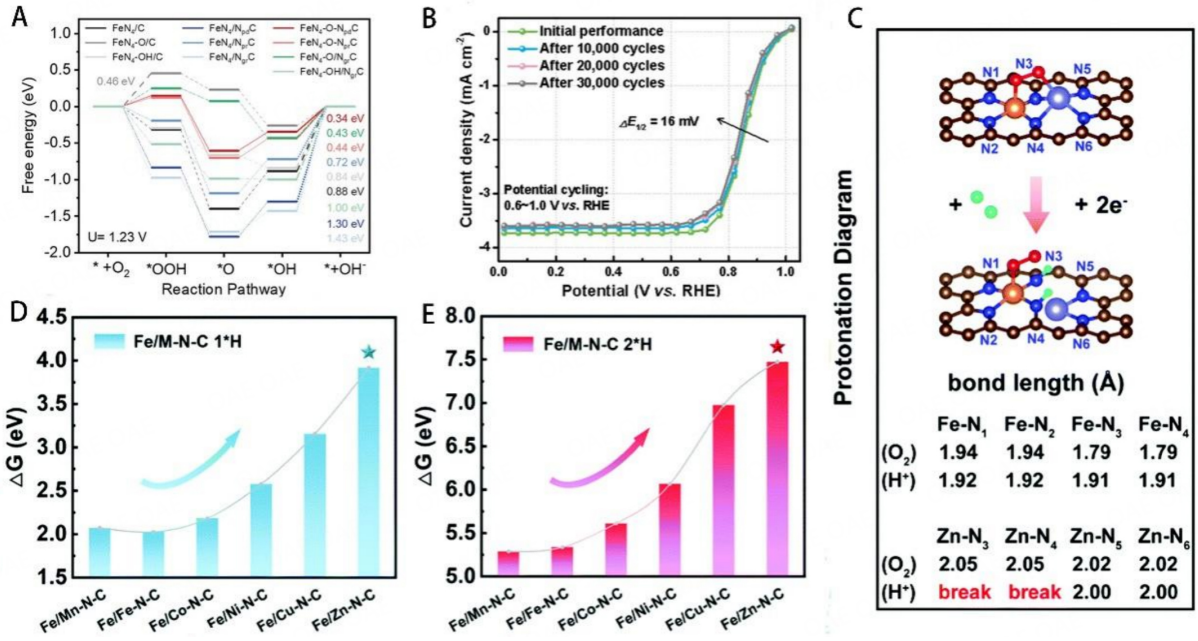

Figure 14. (A) Scaling relationships between the η_{ORR} and d-band center of Fe-3d orbits for the FeN_4-based structures (pd, pr, and gr refer to pyridinic N, pyrrolic N, and graphitic N). This figure is quoted with permission from Peng *et al.*[129]. (B) LSV after different cycles Potential cycling during low-potential range (0.6-1.0 V *vs.* RHE) p-FeNC@CoNC at 25 °C in O_2-saturated 0.5 M H_2SO_4 solution. This figure is quoted with permission from Yang *et al.*[75]. (C) ΔG_{1*H} and (D) ΔG_{2*H} for Fe/M-N-C (M = Mn, Fe, Co, Ni, Cu, and Zn). (E) Protonation diagram of Fe/Zn-N-C. These figures are quoted with permission from Li *et al.*[76].

most Zn-N bonds were broken after protonation. The FeN_4 active centers were protected by the sacrifice of Zn-N bonds [Figure 14E]. Therefore, designing diatomic catalysts was the feasible way to solve the unstable issue of catalysts, including insufficient intrinsic stability, protonation of N-groups, excessive H_2O_2 yield, *etc.*

Water management

Large amounts of active sites are embedded in the micropores; thus, blocking the micropores induce high mass transfer resistance due to the prevention of O_2 and H^+ approach to active sites. Micropore flooding always leads to activity loss of catalysts during the MEA test. Therefore, efficient water management is significant for improving the durability of PGM-free cathode in MEA. Regulating the structure of carbon matrix is a feasible method to alleviate water flooding. The hierarchical porous structure can maximize the effect of catalysts by facilitating mass transfer and alleviating micropore flooding. The introduction of macropores and microporous can offer sufficient water-draining channels for reactants transferring and alleviating micropore flooding. To elucidate the influence microporous layer in water management, Tabe *et al.* developed a freezing method to monitor water distribution on the catalyst layers and further illuminate the influence of microporous layer on the performance of fuel cells and the water content of gas diffusion layers[130]. The water content was further measured by comparing the presence [Figure 15A] and absence of microporous layer [Figure 15B], where the presence of water in the catalyst layers was detected as ice. The interface of catalyst layers and gas diffusion layers provided a space for the accumulation of water. In contrast, the participation of microporous layer could boost water gasification and restrain water accumulation. The enhanced MEA performance also proved the effect of micropores [Figure 15C], which offered a buffer layer for water accumulation.

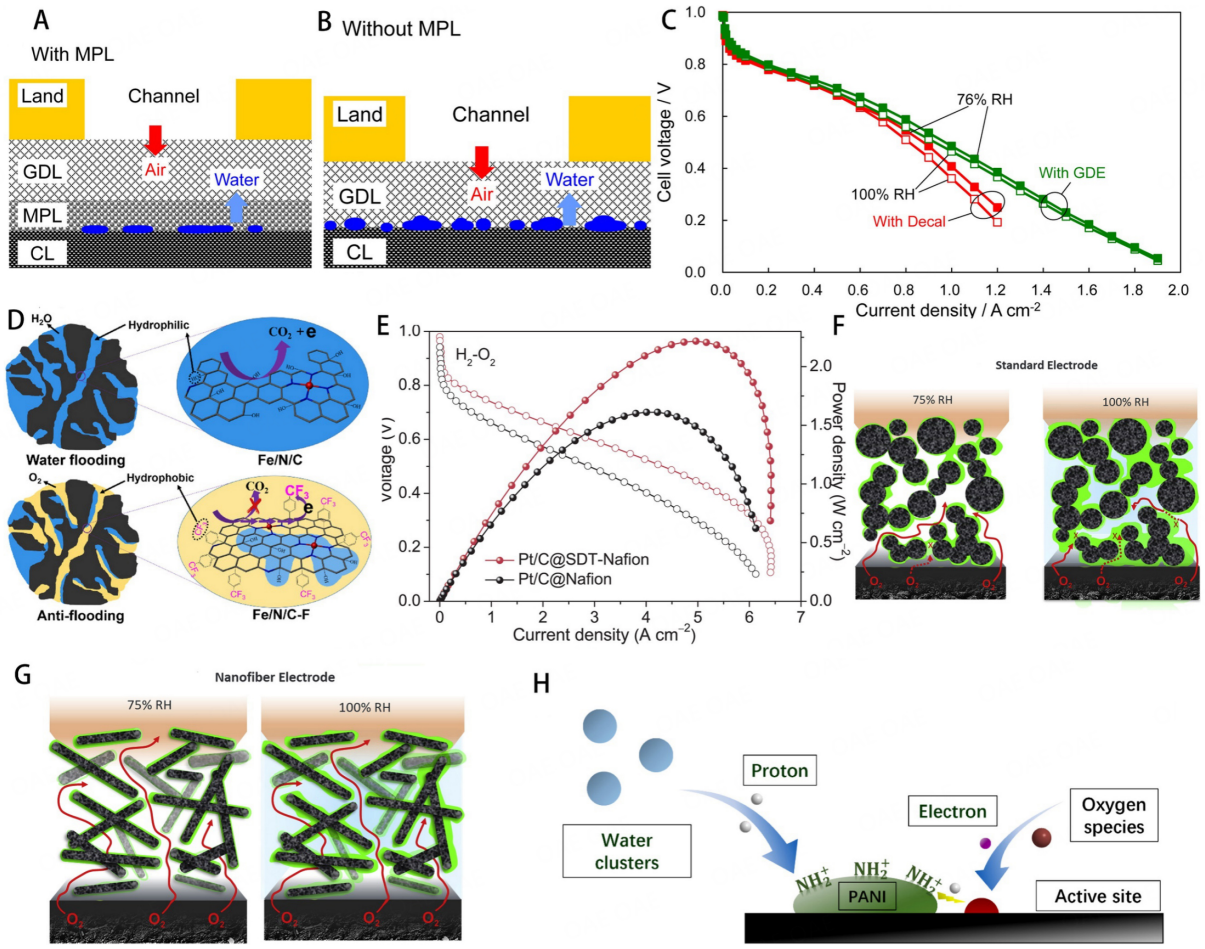

Figure 15. Schematic water distribution on a cathode with (A) or without(B) microporous layer. (C) Polarization curves for the MEAs at 35 °C operations (100% and 76% RH). These figures are quoted with permission from Tabe *et al.*[130]. (D) The hydrophobic group (Ar-CF_3) was modified in Fe-N-C catalysts to boost the resistance to carbon corrosion and water flooding. This figure is quoted with permission from Wang *et al.*[133]. (E) H_2-O_2 PEMFCs polarization and power density curves of the cells with Pt/C@Nafion and Pt/C@SDT-Nafion measured at 80 °C and 100% RH under 150 kPa. This figure is quoted with permission from Zhang *et al.*[134]. (F, G) Schematic representation of ionomer distribution and gas transport at high and low RH in standard and nanofiber electrode layers. These figures are quoted with permission from Kabir *et al*.[135]. (H) Schematic of the improvement of ORR activity caused by the enriched protons. This figure is quoted with permission from Liu *et al.*[136].

The electrocatalytic reaction mainly occurs in the oxygen-water-catalyst three-phase microenvironment. The prevailing strategies for water management include increasing the density of exposed active sites and optimizing the three-phase environment by tailoring the catalyst and Nafion. Modification on carbon matrix surfaces such as -OH, -COOH (hydrophilic functional groups), or heteroatom could change the electronic structure and achieve high intrinsic activity[131]. However, the introduction of hydrophilic function groups can prolong the water retention time in micropores or even block micropores, consequently resulting in high mass transfer resistance and carbon corrosion[132]. If the carbon surface is modified with hydrophobic functional groups, hydrophobic channels can be provided to improve the durability of the catalyst. For example, Wang *et al.* modified the Fe-N-C catalysts with a hydrophobic group (Ar-CF_3) [Figure 15D][133]. Fe-N-C-F catalysts showed a high angle of 165° and kept not-wetting in the contact angles test, while for the pristine Fe-N-C catalysts, the droplet was absorbed too quickly to measure the contact angle. The stability in H_2-O_2 PEMFC was assessed by potentiostatic tests, which showed that the decay of Fe-N-C-F was less than that of pristine Fe-N-C, with only a 15% decay in initial performance after

100 h at 0.6 V. After 40 h of operation at 0.5 V, the content change of Fe was measured by UV-Vis spectrophotometry. The pristine Fe-N-C changed greatly (from 1.8% to 0.38%), while only a slight change of Fe content for Fe-N-C-F (from 1.2% to 1.1%) was observed. The higher hydrophobicity of carbon matrix led to less demetallation of Fe and enhanced stability of catalysts. After introducing the hydrophobic group ($Ar\text{-}CF_3$), the catalyst exhibited high hydrophobicity and enhanced carbon corrosion resistance. The tailoring of the catalyst and Nafion by incorporating hydrophobic functional groups or pore-forming additives can improve gas transport capability. Optimizing the three-phase environment by tailoring the Nafion was also an important strategy for water management. Zhang *et al.* incorporated a sulfonic acid functionalized covalent organic framework (COF) nanosheets with different pore sizes into Nafion, which facilitated the formation of the three-phase interface and improved the mass transfer of O_2[134]. The ultra-high peak power density after water management (2.21 Wcm^{-2}) is 1.4 times higher compared to the performance of the MEA without COF [Figure 15E]. The durability of the fuel cell was also improved significantly, with a low rate of reduction (38%) in mass activity after 30,000 cycles AST, even meeting the DOE's 2025 target (40%). Electrospinning techniques can also be used to promote the mass transport of O_2 and protons. Kabir *et al.* prepared the nanofiber electrode by electrospinning the mixture of Fe-N-C catalyst, Nafion, and Poly Acrylic acid[135]. As shown in Figures 15F and 15G, nanofiber electrodes provided more mass transfer channels than standard electrodes, especially in test conditions with high relative humidity. Our group designed Czif-8-Fe-*x*PANI catalysts modified with polyaniline, which created a protophilic environment on the catalyst surface[136]. Polyaniline can provide enough amine groups to facilitate the release of protons from the water cluster [Figure 15H] and improve the ORR performance, with the half-wave potential of the catalyst increased from 0.815 V to 0.835 V.

In conclusion, water management is an important method of catalytic performance improvement, especially in MEAs.

CONCLUSION AND OUTLOOK

The development of M-N-C catalysts seems like a long journey approaching our ultimate target of commercializing PEMFC. Many attempts were applied to remove the barriers on the way to achieving high activity and stability of catalysts. However, as the activity of M-N-C catalysts approaches that of PGM catalysts, the stability of PGM-free catalysts remains the main obstacle to widespread application. The rational design of excellent PGM-free catalysts remains difficult as the relationship between tuning the structure and improving durability is unclear. With the development of advanced characterization techniques, especially the application of several *in situ* techniques over the past few decades, the identification of active sites has made great strides. Nevertheless, the degradation mechanism of the active site still requires further exploration. In this review, we summarize several possible mechanisms, including carbon corrosion, demetallation, water flooding in micropores, and nitrogen protonation. Several studies proposed that carbon corrosion and demetallation may be the main problems of activity decay. A series of endeavors should focus on overcoming these challenges. Some directions are summarized below:

Advanced *in situ* technology. By monitoring the evolution of the surface structure, the mechanism of the catalysis and degradation processes is partially elucidated. Advanced characterization techniques combined with theoretical calculations can be used to predict and simulate the structural evolution of active sites.

Design a carbon matrix rich in mesopores and macropores. Mesopores and macropores can increase the mass transfer rate and alleviate micropore flooding. The introduction of mesopores and macropores can prevent the active sites embedded in micropores from leaching. The leached active sites in micropores may be the main cause of initial activity loss.

Intrinsic stability improvement of active sites. Building robust M-N bonds has been proven to be a valid method for improving the intrinsic stability of catalysts. Changing the binding constant of the metal center and chelation, as well as changing the ratio of pyridinic N, were successfully used to regulate the bond length of Fe-N, which exceedingly improved the intrinsic stability of catalysts.

Non-carbon-supported catalyst. Severe carbon corrosion is unavoidable and caused by electrochemical oxidation and chemical oxidation. Several non-carbon-based electrocatalysts have been advanced in the past few years, including metal alloys[137], metal oxides[138], metal hydroxides[139], nitrides[140], carbides[141], phosphides[142], metal chalcogenides[143], and microporous materials[144]. The matrix is an essential part of catalysts, providing not only a platform to anchor active sites but also a coordinated environment, which further affects the electron structure of active centers and the durability of catalysts.

In summary, M-N-C catalysts exhibit great potential to replace PGM catalysts in fuel cell technology. Although the durability of M-N-C catalysts is still insufficient for widespread application, the catalytic performance of M-N-C catalysts has dramatically advanced in the past few decades. We hold optimistic opinions and believe that with the development of technology and theoretical knowledge, the current issues of M-N-C catalysts will be solved in the future, realizing the dramatic improvement in MEA performance. In addition to hydrogen fuel cells, M-N-C catalysts have displayed promising performance in CO_2 reduction reactions (CO_2RR)[145,146], hydrogen evolution reaction (HER)[147,148], nitrogen reduction reactions (NRR)[149,150] and microbial fuel cell (MFC)[151-154]. M-N-C catalysts play special roles in electrochemical energy conversion and storage.

DECLARATIONS

Authors' contributions

Prepared the manuscript: Wang S, Chu Y, Lan C
Performed manuscript correcting: Liu C, Ge J, Xing W

Availability of data and materials

Not applicable.

Financial support and sponsorship

The work was supported by the National Natural Science Foundation of China (21633008, 21875243, U1601211), National Science and Technology Major Project (2016YFB0101202), Jilin Province Science and Technology Development Program (20200201001JC, 20190201270JC, 20180101030JC).

Conflicts of interest

All authors declared that there are no conflicts of interest.

Ethical approval and consent to participate

Not applicable.

Consent for publication

Not applicable.

REFERENCES

1. Shih CF, Zhang T, Li J, Bai C. Powering the future with liquid sunshine. *Joule* 2018;2:1925-49. DOI
2. Debe MK. Electrocatalyst approaches and challenges for automotive fuel cells. *Nature* 2012;486:43-51. DOI PubMed
3. Hou J, Yang M, Ke C, et al. Platinum-group-metal catalysts for proton exchange membrane fuel cells: from catalyst design to electrode structure optimization. *EnergyChem* 2020;2:100023. DOI
4. Moloudi M, Noori A, Rahmanifar MS, et al. Layered double hydroxide templated synthesis of amorphous NiCoFeB as a multifunctional electrocatalyst for overall water splitting and rechargeable Zinc–Air batteries. *Adv Funct Mater* 2023;13:2203002. DOI
5. Cui P, Zhao L, Long Y, Dai L, Hu C. Carbon-based electrocatalysts for acidic oxygen reduction reaction. *Angew Chem Int Ed Engl* 2023:e202218269. DOI PubMed
6. Xu MJ, Ge JJ, Liu CP, Xing W. Research progress of metal-nitrogen-carbon catalysts toward oxygen reduction reaction in changchun institute of applied chemistry. *J Electrochem* 2020;26:464-73. DOI
7. Li Y, Pillai HS, Wang T, et al. High-performance ammonia oxidation catalysts for anion-exchange membrane direct ammonia fuel cells. *Energy Environ Sci* 2021;14:1449-60. DOI
8. Li X, He Y, Cheng S, et al. Atomic structure evolution of pt-co binary catalysts: single metal sites versus intermetallic nanocrystals. *Adv Mater* 2021;33:e2106371. DOI PubMed
9. Wan X, Liu X, Li Y, et al. Fe–N–C electrocatalyst with dense active sites and efficient mass transport for high-performance proton exchange membrane fuel cells. *Nat Catal* 2019;2:259-68. DOI
10. Jasinski R. A new fuel cell cathode catalyst. *Nature* 1964;201:1212-3. DOI
11. Lefèvre M, Proietti E, Jaouen F, Dodelet JP. Iron-based catalysts with improved oxygen reduction activity in polymer electrolyte fuel cells. *Science* 2009;324:71-4. DOI PubMed
12. Proietti E, Jaouen F, Lefèvre M, et al. Iron-based cathode catalyst with enhanced power density in polymer electrolyte membrane fuel cells. *Nat Commun* 2011;2:416. DOI PubMed
13. Wu G, More KL, Johnston CM, Zelenay P. High-performance electrocatalysts for oxygen reduction derived from polyaniline, iron, and cobalt. *Science* 2011;332:443-7. DOI PubMed
14. Zhang H, Chung HT, Cullen DA, et al. High-performance fuel cell cathodes exclusively containing atomically dispersed iron active sites. *Energy Environ Sci* 2019;12:2548-58. DOI
15. Department of Energy. Advanced PGM-free cathode engineering for high power density and durability; 2021. Available from: https://www.hydrogen.energy.gov/pdfs/review21/fc171_litster_2021_o.pdf [Last accessed on 08 Aug 2022]. DOI
16. Liu Q, Liu X, Zheng L, Shui J. The solid-phase synthesis of an Fe-N-C electrocatalyst for high-power proton-exchange membrane fuel cells. *Angew Chem Int Ed Engl* 2018;57:1204-8. DOI PubMed
17. Du L, Prabhakaran V, Xie X, Park S, Wang Y, Shao Y. Low-PGM and PGM-free catalysts for proton exchange membrane fuel cells: stability challenges and material solutions. *Adv Mater* 2021;33:e1908232. DOI PubMed
18. Shao Y, Dodelet JP, Wu G, Zelenay P. PGM-free cathode catalysts for PEM fuel cells: a mini-review on stability challenges. *Adv Mater* 2019;31:e1807615. DOI PubMed
19. Miao Z, Li S, Priest C, Wang T, Wu G, Li Q. Effective approaches for designing stable M-N(x) /C oxygen-reduction catalysts for proton-exchange-membrane fuel cells. *Adv Mater* 2022;34:e2200595. DOI PubMed
20. Banham D, Kishimoto T, Zhou Y, et al. Critical advancements in achieving high power and stable nonprecious metal catalyst-based MEAs for real-world proton exchange membrane fuel cell applications. *Sci Adv* 2018;4:eaar7180. DOI PubMed PMC
21. Liu J, Sun X, Song P, Zhang Y, Xing W, Xu W. High-performance oxygen reduction electrocatalysts based on cheap carbon black, nitrogen, and trace iron. *Adv Mater* 2013;25:6879-83. DOI PubMed
22. Xie X, He C, Li B, et al. Performance enhancement and degradation mechanism identification of a single-atom Co–N–C catalyst for proton exchange membrane fuel cells. *Nat Catal* 2020;3:1044-54. DOI
23. Cheng Q, Yang L, Zou L, et al. Single cobalt atom and N codoped carbon nanofibers as highly durable electrocatalyst for oxygen reduction reaction. *ACS Catal* 2017;7:6864-71. DOI
24. Qu Y, Li Z, Chen W, et al. Direct transformation of bulk copper into copper single sites via emitting and trapping of atoms. *Nat Catal* 2018;1:781-6. DOI
25. Luo E, Zhang H, Wang X, et al. Single-atom Cr-N(4) sites designed for durable oxygen reduction catalysis in acid media. *Angew Chem Int Ed Engl* 2019;58:12469-75. DOI PubMed
26. Li J, Chen M, Cullen DA, et al. Atomically dispersed manganese catalysts for oxygen reduction in proton-exchange membrane fuel cells. *Nat Catal* 2018;1:935-45. DOI
27. Wang L, Zhang J, Zheng L, et al. Carbon black-supported FM–N–C (FM = Fe, Co, and Ni) single-atom catalysts synthesized by the self-catalysis of oxygen-coordinated ferrous metal atoms. *J Mater Chem A* 2020;8:13166-72. DOI
28. He Y, Liu S, Priest C, Shi Q, Wu G. Atomically dispersed metal-nitrogen-carbon catalysts for fuel cells: advances in catalyst design, electrode performance, and durability improvement. *Chem Soc Rev* 2020;49:3484-524. DOI PubMed
29. Choi CH, Choi WS, Kasian O, et al. Unraveling the nature of sites active toward hydrogen peroxide reduction in Fe-N-C catalysts. *Angew Chem Int Ed Engl* 2017;56:8809-12. DOI PubMed PMC
30. Liu M, Wang L, Zhao K, et al. Atomically dispersed metal catalysts for the oxygen reduction reaction: synthesis, characterization, reaction mechanisms and electrochemical energy applications. *Energy Environ Sci* 2019;12:2890-923. DOI

31. Singh H, Zhuang S, Ingis B, Nunna BB, Lee ES. Carbon-based catalysts for oxygen reduction reaction: A review on degradation mechanisms. *Carbon* 2019;151:160-74. DOI
32. Duan Z, Wang G. A first principles study of oxygen reduction reaction on a Pt(111) surface modified by a subsurface transition metal M (M = Ni, Co, or Fe). *Phys Chem Chem Phys* 2011;13:20178-87. DOI
33. Han Y, Wang Y, Xu R, et al. Electronic structure engineering to boost oxygen reduction activity by controlling the coordination of the central metal. *Energy Environ Sci* 2018;11:2348-52. DOI
34. Ramaswamy N, Tylus U, Jia Q, Mukerjee S. Activity descriptor identification for oxygen reduction on nonprecious electrocatalysts: linking surface science to coordination chemistry. *J Am Chem Soc* 2013;135:15443-9. DOI PubMed
35. Mun Y, Lee S, Kim K, et al. Versatile strategy for tuning ORR activity of a single Fe-N(4) site by controlling electron-withdrawing/donating properties of a carbon plane. *J Am Chem Soc* 2019;141:6254-62. DOI PubMed
36. Ramaswamy N, Mukerjee S. Influence of inner- and outer-sphere electron transfer mechanisms during electrocatalysis of oxygen reduction in alkaline media. *J Phys Chem C* 2011;115:18015-26. DOI
37. Wang X, Liu CP, Ge JJ, Zhu JB, Xing W. Recent advances in structural regulation on non-precious metal catalysts for oxygen reduction reaction in alkaline electrolytes. *J Electrochem* 2022;28:2108501. DOI
38. Mustain WE, Chatenet M, Page M, Kim YS. Durability challenges of anion exchange membrane fuel cells. *Energy Environ Sci* 2020;13:2805-38. DOI
39. Jiang WJ, Gu L, Li L, et al. Understanding the high activity of Fe-N-C electrocatalysts in oxygen reduction: Fe/Fe3C nanoparticles boost the activity of Fe-N(x). *J Am Chem Soc* 2016;138:3570-8. DOI PubMed
40. Chung Hoon T, Cullen David A, Higgins D, et al. Direct atomic-level insight into the active sites of a high-performance PGM-free ORR catalyst. *Science* 2017;357:479-84. DOI PubMed
41. Lefèvre M, Dodelet JP, Bertrand P. Molecular oxygen reduction in pem fuel cells: evidence for the simultaneous presence of two active sites in Fe-based catalysts. *J Phys Chem B* 2002;106:8705-13. DOI
42. Shah SSA, Najam T, Bashir MS, et al. Identification of catalytic active sites for durable proton exchange membrane fuel cell: catalytic degradation and poisoning perspectives. *Small* 2022;18:e2106279. DOI PubMed
43. Li J, Sougrati MT, Zitolo A, et al. Identification of durable and non-durable FeNx sites in Fe–N–C materials for proton exchange membrane fuel cells. *Nat Catal* 2021;4:10-9. DOI
44. Xu X, Zhang X, Kuang Z, et al. Investigation on the demetallation of Fe-N-C for oxygen reduction reaction: the influence of structure and structural evolution of active site. *Appl Catal* ;309:121290. DOI
45. Mineva T, Matanovic I, Atanassov P, et al. Understanding active sites in pyrolyzed Fe–N–C catalysts for fuel cell cathodes by bridging density functional theory calculations and ^{57}Fe mössbauer spectroscopy. *ACS Catal* 2019;9:9359-71. DOI
46. Liu S, Li C, Zachman MJ, et al. Atomically dispersed iron sites with a nitrogen–carbon coating as highly active and durable oxygen reduction catalysts for fuel cells. *Nat Energy* 2022;7:652-63. DOI
47. Department of energy. electrocat: durable Mn-based PGM-free catalysts for polymer electrolyte membrane fuel cells; 2021. Available from: https://www.hydrogen.energy.gov/pdfs/review21/fc170_xu_2021_o.pdf [Last accessed on 01 Feb Aug 2023]. DOI
48. He Y, Wu G. PGM-free oxygen-reduction catalyst development for proton-exchange membrane fuel cells: challenges, solutions, and promises. *Acc Mater Res* 2022;3:224-36. DOI
49. Kocha SS, Shinozaki K, Zack JW, et al. Best practices and testing protocols for benchmarking ORR activities of fuel cell electrocatalysts using rotating disk electrode. *Electrocatalysis* 2017;8:366-74. DOI
50. Kong F, Cui X, Huang Y, et al. N-doped carbon electrocatalyst: marked ORR activity in acidic media without the contribution from metal sites? *Angew Chem Int Ed Engl* 2022;61:e202116290. DOI PubMed
51. Zhao YX, Wen JH, Li P, et al. A "pre-division metal clusters" strategy to mediate efficient dual-active sites ORR catalyst for ultralong rechargeable ZN-air battery. *Angew Chem Int Ed Engl* 2023;62:e202216950. DOI
52. Lazaridis T, Stühmeier BM, Gasteiger HA, El-sayed HA. Capabilities and limitations of rotating disk electrodes versus membrane electrode assemblies in the investigation of electrocatalysts. *Nat Catal* 2022;5:363-73. DOI
53. Beltrán DE, Litster S. Half-wave potential or mass activity? *ACS Energy Lett* 2019;4:1158-61. DOI
54. Martens S, Asen L, Ercolano G, et al. A comparison of rotating disc electrode, floating electrode technique and membrane electrode assembly measurements for catalyst testing. *Jops* 2018;392:274-84. DOI
55. Jaouen F, Herranz J, Lefèvre M, et al. Cross-laboratory experimental study of non-noble-metal electrocatalysts for the oxygen reduction reaction. *ACS Appl Mater Interfaces* 2009;1:1623-39. DOI PubMed
56. Zhu Y, Sokolowski J, Song X, He Y, Mei Y, Wu G. Engineering local coordination environments of atomically dispersed and heteroatom-coordinated single metal site electrocatalysts for clean energy-conversion. *Adv Energy Mater* 2020;10:1902844. DOI
57. Shi Q, Hwang S, Yang H, et al. Supported and coordinated single metal site electrocatalysts. Mater Today 2020;37:93-111. DOI
58. Suntivich J, Gasteiger HA, Yabuuchi N, Shao-horn Y. Electrocatalytic measurement methodology of oxide catalysts using a thin-film rotating disk electrode. *J Electrochem Soc* 2010;157:B1263. DOI
59. Hu X, Chen S, Chen L, et al. What is the real origin of the activity of Fe-N-C electrocatalysts in the O(2) reduction reaction? *J Am Chem Soc* 2022;144:18144-52. DOI PubMed
60. Liu J, Talarposhti MR, Asset T, et al. Understanding the role of interfaces for water management in platinum group metal-free electrodes in polymer electrolyte fuel cells. *ACS Appl Energy Mater* 2019;2:3542-53. DOI
61. Ito H, Maeda T, Nakano A, Takenaka H. Properties of nafion membranes under PEM water electrolysis conditions. Int J Hydrogen

Energy 2011;36:10527-40. DOI
62. Primbs M, Sun Y, Roy A, et al. Establishing reactivity descriptors for platinum group metal (PGM)-free Fe–N–C catalysts for PEM fuel cells. *Energy Environ Sci* 2020;13:2480-500. DOI
63. Mehmood A, Gong M, Jaouen F, et al. High loading of single atomic iron sites in Fe–NC oxygen reduction catalysts for proton exchange membrane fuel cells. *Nat Catal* 2022;5:311-23. DOI
64. Stariha S, Macauley N, Sneed BT, et al. Recent advances in catalyst accelerated stress tests for polymer electrolyte membrane fuel cells. *J Electrochem Soc* 2018;165:F492-501. DOI
65. Osmieri L, Cullen DA, Chung HT, Ahluwalia RK, Neyerlin K. Durability evaluation of a Fe-N-C catalyst in polymer electrolyte fuel cell environment via accelerated stress tests. *Nano Energy* 2020;78:105209. DOI
66. Zhang H, Osmieri L, Park JH, et al. Standardized protocols for evaluating platinum group metal-free oxygen reduction reaction electrocatalysts in polymer electrolyte fuel cells. *Nat Catal* 2022;5:455-62. DOI
67. Miao Z, Wang X, Zhao Z, et al. Improving the stability of non-noble-metal M-N-C catalysts for proton-exchange-membrane fuel cells through M-N bond length and coordination regulation. *Adv Mater* 2021;33:e2006613. DOI PubMed
68. Chen G, An Y, Liu S, et al. Highly accessible and dense surface single metal FeN_4 active sites for promoting the oxygen reduction reaction. *Energy Environ Sci* 2022;15:2619-28. DOI
69. Li L, Wen Y, Han G, et al. Tailoring the stability of Fe-N-C via pyridinic nitrogen for acid oxygen reduction reaction. Chem Eng J 2022;437:135320. DOI
70. He Y, Hwang S, Cullen DA, et al. Highly active atomically dispersed CoN_4 fuel cell cathode catalysts derived from surfactant-assisted MOFs: carbon-shell confinement strategy. *Energy Environ Sci* 2019;12:250-60. DOI
71. Xiao M, Zhang H, Chen Y, et al. Identification of binuclear Co2N5 active sites for oxygen reduction reaction with more than one magnitude higher activity than single atom CoN4 site. *Nano Energy* 2018;46:396-403. DOI
72. Wan X, Liu Q, Liu J, et al. Iron atom-cluster interactions increase activity and improve durability in Fe-N-C fuel cells. *Nat Commun* 2022;13:2963. DOI PubMed PMC
73. Liu S, Wang M, Yang X, et al. Chemical vapor deposition for atomically dispersed and nitrogen coordinated single metal site catalysts. *Angew Chem Int Ed Engl* 2020;59:21698-705. DOI PubMed
74. Li W, Liu B, Liu D, et al. Alloying co species into ordered and interconnected macroporous carbon polyhedra for efficient oxygen reduction reaction in rechargeable zinc-air batteries. *Adv Mater* 2022;34:e2109605. DOI PubMed
75. Yang X, Wang M, Zachman MJ, et al. Binary atomically dispersed metal-site catalysts with core−shell nanostructures for O_2 and CO_2 reduction reactions. *Small Science* 2021;1:2100046. DOI
76. Li H, Di S, Niu P, Wang S, Wang J, Li L. A durable half-metallic diatomic catalyst for efficient oxygen reduction. *Energy Environ Sci* 2022;15:1601-10. DOI
77. Yan Z, Zhang Y, Jiang Z, Jiang D, Wei W, Hu Z. Nitrogen-doped bimetallic carbide-graphite composite as highly active and extremely stable electrocatalyst for oxygen reduction reaction in alkaline media. *Adv Funct Materials* 2022;32:2204031. DOI
78. Xie H, Xie X, Hu G, et al. Ta–TiOx nanoparticles as radical scavengers to improve the durability of Fe–N–C oxygen reduction catalysts. *Nat Energy* 2022;7:281-9. DOI
79. He T, Chen Y, Liu Q, et al. Theory-guided regulation of FeN(4) spin state by neighboring Cu atoms for enhanced oxygen reduction electrocatalysis in flexible metal-air batteries. *Angew Chem Int Ed Engl* 2022;61:e202201007. DOI PubMed
80. Xiao M, Chen Y, Zhu J, et al. Climbing the apex of the ORR volcano plot via binuclear site construction: electronic and geometric engineering. *J Am Chem Soc* 2019;141:17763-70. DOI PubMed
81. Yin S, Yang S, Li G, et al. Seizing gaseous Fe^{2+} to densify O_2-accessible $Fe\text{-}N_4$ sites for high-performance proton exchange membrane fuel cells. *Energy Environ Sci* 2022;15:3033-40. DOI
82. Han G, Zheng Y, Zhang X, et al. High loading single-atom Cu dispersed on graphene for efficient oxygen reduction reaction. *Nano Energy* 2019;66:104088. DOI
83. Luo F, Roy A, Silvioli L, et al. P-block single-metal-site tin/nitrogen-doped carbon fuel cell cathode catalyst for oxygen reduction reaction. *Nat Mater* 2020;19:1215-23. DOI
84. Shi Z, Kallenbach NR. Ramachandran redux. *Proc Natl Acad Sci USA* 2011;108:3-4. DOI PubMed PMC
85. Bligaard T, Nørskov J. Ligand effects in heterogeneous catalysis and electrochemistry. Electrochim Acta 2007;52:5512-6. DOI
86. Xu H, Cheng D, Cao D, Zeng XC. A universal principle for a rational design of single-atom electrocatalysts. *Nat Catal* 2018;1:339-48. DOI
87. Kulkarni A, Siahrostami S, Patel A, Nørskov JK. Understanding Catalytic Activity Trends in the Oxygen Reduction Reaction. *Chem Rev* 2018;118:2302-12. DOI PubMed
88. Man IC, Su H, Calle-vallejo F, et al. Universality in oxygen evolution electrocatalysis on oxide surfaces. *ChemCatChem* 2011;3:1159-65. DOI
89. Zagal JH, Koper MT. Reactivity descriptors for the activity of molecular MN4 catalysts for the oxygen reduction reaction. *Angew Chem Int Ed Engl* 2016;55:14510-21. DOI PubMed
90. Luo E, Chu Y, Liu J, et al. Pyrolyzed $M–N_x$ catalysts for oxygen reduction reaction: progress and prospects. *Energy Environ Sci* 2021;14:2158-85. DOI
91. Chen L, Yu W, Wang T, et al. Fluorescence detection of hydroxyl radical generated from oxygen reduction on Fe/N/C catalyst. *Sci China Chem* 2020;63:198-202. DOI

92. Martinaiou I, Shahraei A, Grimm F, et al. Effect of metal species on the stability of Me-N-C catalysts during accelerated stress tests mimicking the start-up and shut-down conditions. *Electrochim Acta* 2017;243:183-96. DOI
93. Yu Y, Li H, Wang H, Yuan X, Wang G, Pan M. A review on performance degradation of proton exchange membrane fuel cells during startup and shutdown processes: Causes, consequences, and mitigation strategies. *Jops* 2012;205:10-23. DOI
94. Kumar K, Dubau L, Mermoux M, et al. On the influence of oxygen on the degradation of Fe-N-C catalysts. *Angew Chem Int Ed Engl* 2020;59:3235-43. DOI PubMed
95. Choi CH, Lim H, Chung MW, et al. The achilles' heel of iron-based catalysts during oxygen reduction in an acidic medium. *Energy Environ Sci* 2018;11:3176-82. DOI
96. Chung HT, Won JH, Zelenay P. Active and stable carbon nanotube/nanoparticle composite electrocatalyst for oxygen reduction. *Nat Commun* 2013;4:1922. DOI PubMed PMC
97. Choi CH, Baldizzone C, Polymeros G, et al. Minimizing operando demetallation of Fe-N-C electrocatalysts in acidic medium. *ACS Catal* 2016;6:3136-46. DOI
98. Ku YP, Ehelebe K, Hutzler A, et al. Oxygen Reduction reaction in alkaline media causes iron leaching from Fe-N-C electrocatalysts. *J Am Chem Soc* 2022;144:9753-63. DOI PubMed
99. Wan X, Shui J. Exploring durable single-atom catalysts for proton exchange membrane fuel cells. *ACS Energy Lett* 2022;7:1696-705. DOI
100. Li J, Chen S, Yang N, et al. Ultrahigh-loading zinc single-atom catalyst for highly efficient oxygen reduction in both acidic and alkaline media. *Angew Chem Int Ed Engl* 2019;58:7035-9. DOI PubMed
101. Yang N, Peng L, Li L, et al. Theoretically probing the possible degradation mechanisms of an FeNC catalyst during the oxygen reduction reaction. *Chem Sci* 2021;12:12476-84. DOI PubMed PMC
102. Herranz J, Jaouen F, Lefèvre M, et al. Unveiling N-protonation and anion-binding effects on Fe/N/C-catalysts for O(2) reduction in PEM fuel cells. *J Phys Chem C Nanomater Interfaces* 2011;115:16087-97. DOI PubMed PMC
103. Li H, Tang Y, Wang Z, et al. A review of water flooding issues in the proton exchange membrane fuel cell. *Jops* 2008;178:103-17. DOI
104. Fu X, Zamani P, Choi JY, et al. In situ polymer graphenization ingrained with nanoporosity in a nitrogenous electrocatalyst boosting the performance of polymer-electrolyte-membrane fuel cells. *Adv Mater* 2017;29:1604456. DOI PubMed
105. Choi J, Yang L, Kishimoto T, et al. Is the rapid initial performance loss of Fe/N/C non precious metal catalysts due to micropore flooding? *Energy Environ Sci* 2017;10:296-305. DOI
106. Xia D, Yang X, Xie L, et al. Direct growth of carbon nanotubes doped with single atomic Fe-N $_4$ active sites and neighboring graphitic nitrogen for efficient and stable oxygen reduction electrocatalysis. *Adv Funct Mater* 2019;29:1906174. DOI
107. Ma Q, Jin H, Zhu J, et al. Stabilizing Fe-N-C catalysts as model for oxygen reduction reaction. *Adv Sci (Weinh)* 2021;8:e2102209. DOI PubMed PMC
108. Qu X, Han Y, Chen Y, et al. Stepwise pyrolysis treatment as an efficient strategy to enhance the stability performance of Fe-NX/C electrocatalyst towards oxygen reduction reaction and proton exchange membrane fuel cell. *Appl Catal* 2021;295:120311. DOI
109. Yoo JM, Shin H, Chung DY, Sung YE. Carbon shell on active nanocatalyst for stable electrocatalysis. *Acc Chem Res* 2022;55:1278-89. DOI PubMed
110. Kim K, Min K, Go Y, et al. FeCo alloy nanoparticles embedded in N-doped carbon supported on highly defective ketjenblack as effective bifunctional electrocatalysts for rechargeable Zn–air batteries. *Appl Catal* 2022;315:121501. DOI
111. Ohyama J, Moriya M, Takahama R, et al. High durability of a 14-membered hexaaza macrocyclic fe complex for an acidic oxygen reduction reaction revealed by in situ XAS analysis. *JACS Au* 2021;1:1798-804. DOI PubMed PMC
112. Li J, Zhang H, Samarakoon W, et al. Thermally driven structure and performance evolution of atomically dispersed FeN(4) sites for oxygen reduction. *Angew Chem Int Ed Engl* 2019;58:18971-80. DOI PubMed
113. Ye W, Chen S, Lin Y, et al. Precisely tuning the number of fe atoms in clusters on N-doped carbon toward acidic oxygen reduction reaction. *Chem* 2019;5:2865-78. DOI
114. Yin SH, Yang J, Han Y, et al. Construction of highly active metal-containing nanoparticles and FeCo-N(4) composite sites for the acidic oxygen reduction reaction. *Angew Chem Int Ed Engl* 2020;59:21976-9. DOI PubMed
115. Liu H, Jiang L, Khan J, et al. Decorating single-atomic Mn sites with FeMn clusters to boost oxygen reduction reaction. *Angew Chem Int Ed Engl* 2023;62:e202214988. DOI PubMed
116. Choi CH, Baldizzone C, Grote JP, Schuppert AK, Jaouen F, Mayrhofer KJ. Stability of Fe-N-C catalysts in acidic medium studied by operando spectroscopy. *Angew Chem Int Ed Engl* 2015;54:12753-7. DOI PubMed
117. Wang Y, Tang YJ, Zhou K. Self-adjusting activity induced by intrinsic reaction intermediate in Fe-N-C single-atom catalysts. *J Am Chem Soc* 2019;141:14115-9. DOI PubMed
118. Xiao M, Gao L, Wang Y, et al. Engineering energy level of metal center: ru single-atom site for efficient and durable oxygen reduction catalysis. *J Am Chem Soc* 2019;141:19800-6. DOI PubMed
119. Wei J, Xia D, Wei Y, Zhu X, Li J, Gan L. Probing the oxygen reduction reaction intermediates and dynamic active site structures of molecular and pyrolyzed Fe–N–C electrocatalysts by in situ raman spectroscopy. *ACS Catal* 2022;12:7811-20. DOI
120. Chen Z, Jiang S, Kang G, Nguyen D, Schatz GC, Van Duyne RP. Operando characterization of iron phthalocyanine deactivation during oxygen reduction reaction using electrochemical tip-enhanced raman spectroscopy. *J Am Chem Soc* 2019;141:15684-92. DOI PubMed

121. Nematollahi P, Barbiellini B, Bansil A, et al. Identification of a robust and durable FeN $_4$ C x catalyst for ORR in PEM fuel cells and the role of the fifth ligand. *ACS Catal* 2022;12:7541-9. DOI
122. Goellner V, Armel V, Zitolo A, Fonda E, Jaouen F. Degradation by hydrogen peroxide of metal-nitrogen-carbon catalysts for oxygen reduction. *J Electrochem Soc* 2015;162:H403-14. DOI
123. Wang Z, Tang H, Zhang H, et al. Synthesis of Nafion/CeO_2 hybrid for chemically durable proton exchange membrane of fuel cell. *J Membr Sci* 2012;421-422:201-10. DOI
124. Yoon KR, Lee KA, Jo S, et al. Mussel-Inspired polydopamine-treated reinforced composite membranes with self-supported CeO x radical scavengers for highly stable PEM fuel cells. *Adv Funct Mater* 2019;29:1806929. DOI
125. Wei H, Su X, Liu J, et al. A CeO_2 modified phenylenediamine-based Fe/N/C with enhanced durability/stability as non-precious metal catalyst for oxygen reduction reaction. *Electrochem Commun* 2018;88:19-23. DOI
126. Zhang L, Guo X, Zhang S, Huang S. Building up the "genome" of bi-atom catalysts toward efficient HER/OER/ORR. *J Mater Chem A* 2022;10:11600-12. DOI
127. Liu Y, Liu X, Lv Z, et al. Tuning the spin state of the iron center by bridge-bonded Fe-O-Ti ligands for enhanced oxygen reduction. *Angew Chem Int Ed Engl* 2022;61:e202117617. DOI PubMed
128. Gong L, Zhang H, Wang Y, et al. Bridge bonded oxygen ligands between approximated FeN(4) sites confer catalysts with high ORR performance. *Angew Chem Int Ed Engl* 2020;59:13923-8. DOI PubMed
129. Peng L, Yang J, Yang Y, et al. Mesopore-rich Fe-N-C catalyst with FeN(4)-O-NC single-atom sites delivers remarkable oxygen reduction reaction performance in alkaline media. *Adv Mater* 2022;34:e2202544. DOI PubMed
130. Tabe Y, Aoyama Y, Kadowaki K, Suzuki K, Chikahisa T. Impact of micro-porous layer on liquid water distribution at the catalyst layer interface and cell performance in a polymer electrolyte membrane fuel cell. *Jops* 2015;287:422-30. DOI
131. Wang XX, Swihart MT, Wu G. Achievements, challenges and perspectives on cathode catalysts in proton exchange membrane fuel cells for transportation. *Nat Catal* 2019;2:578-89. DOI
132. Forouzandeh F, Li X, Banham DW, et al. Improving the corrosion resistance of proton exchange membrane fuel cell carbon supports by pentafluorophenyl surface functionalization. *Jops* 2018;378:732-41. DOI
133. Wang Y, Zhu P, Yang H, et al. Surface fluorination to boost the stability of the Fe/N/C cathode in proton exchange membrane fuel cells. *ChemElectroChem* 2018;5:1914-21. DOI
134. Zhang Q, Dong S, Shao P, et al. Covalent organic framework-based porous ionomers for high-performance fuel cells. *Science* 2022;378:181-6. DOI PubMed
135. Kabir S, Medina S, Wang G, Bender G, Pylypenko S, Neyerlin K. Improving the bulk gas transport of Fe-N-C platinum group metal-free nanofiber electrodes via electrospinning for fuel cell applications. *Nano Energy* 2020;73:104791. DOI
136. Liu J, Ma R, Chu Y, et al. Construction and regulation of a surface protophilic environment to enhance oxygen reduction reaction electrocatalytic activity. *ACS Appl Mater Interfaces* 2020;12:41269-76. DOI PubMed
137. Xia Z, Guo S. Strain engineering of metal-based nanomaterials for energy electrocatalysis. *Chem Soc Rev* 2019;48:3265-78. DOI PubMed
138. Zhao Q, Yan Z, Chen C, Chen J. Spinels: controlled preparation, oxygen reduction/evolution reaction application, and beyond. *Chem Rev* 2017;117:10121-211. DOI PubMed
139. Jin H, Guo C, Liu X, et al. Emerging two-dimensional nanomaterials for electrocatalysis. *Chem Rev* 2018;118:6337-408. DOI PubMed
140. Deng C, He R, Shen W, Li M, Zhang T. A single-atom catalyst of cobalt supported on a defective two-dimensional boron nitride material as a promising electrocatalyst for the oxygen reduction reaction: a DFT study. *Phys Chem Chem Phys* 2019;21:6900-7. DOI PubMed
141. Zhang RQ, Lee TH, Yu BD, Stampfl C, Soon A. The role of titanium nitride supports for single-atom platinum-based catalysts in fuel cell technology. *Phys Chem Chem Phys* 2012;14:16552-7. DOI PubMed
142. Wang X, Bai L, Lu J, et al. Rapid activation of platinum with black phosphorus for efficient hydrogen evolution. *Angew Chem Int Ed Engl* 2019;58:19060-6. DOI PubMed
143. Zhang Y, Zhou Q, Zhu J, Yan Q, Dou SX, Sun W. Nanostructured metal chalcogenides for energy storage and electrocatalysis. *Adv Funct Mater* 2017;27:1702317. DOI
144. Wang HF, Chen L, Pang H, Kaskel S, Xu Q. MOF-derived electrocatalysts for oxygen reduction, oxygen evolution and hydrogen evolution reactions. *Chem Soc Rev* 2020;49:1414-48. DOI PubMed
145. Wang XX, Hwang S, Pan YT, et al. Ordered Pt_3Co intermetallic nanoparticles derived from metal-organic frameworks for oxygen reduction. *Nano Lett* 2018;18:4163-71. DOI PubMed
146. Pan F, Li B, Sarnello E, et al. Boosting CO_2 reduction on Fe-N-C with sulfur incorporation: synergistic electronic and structural engineering. *Nano Energy* 2020;68:104384. DOI
147. Wang ZL, Hao XF, Jiang Z, et al. C and N hybrid coordination derived Co-C-N complex as a highly efficient electrocatalyst for hydrogen evolution reaction. *J Am Chem Soc* 2015;137:15070-3. DOI PubMed
148. Zou X, Huang X, Goswami A, et al. Cobalt-embedded nitrogen-rich carbon nanotubes efficiently catalyze hydrogen evolution reaction at all pH values. *Angew Chem Int Ed Engl* 2014;53:4372-6. DOI PubMed
149. Liu X, Jiao Y, Zheng Y, Jaroniec M, Qiao SZ. Building up a picture of the electrocatalytic nitrogen reduction activity of transition metal single-atom catalysts. *J Am Chem Soc* 2019;141:9664-72. DOI PubMed

150. Mukherjee S, Cullen DA, Karakalos S, et al. Metal-organic framework-derived nitrogen-doped highly disordered carbon for electrochemical ammonia synthesis using N2 and H2O in alkaline electrolytes. *Nano Energy* 2018;48:217-26. DOI
151. Cao B, Zhao Z, Peng L, et al. Silver nanoparticles boost charge-extraction efficiency in Shewanella microbial fuel cells. *Science* 2021;373:1336-40. DOI PubMed
152. Koo B, Jung SP. Improvement of air cathode performance in microbial fuel cells by using catalysts made by binding metal-organic framework and activated carbon through ultrasonication and solution precipitation. *Chem Eng J* 2021;424:130388. DOI
153. Jung S, Regan JM. Influence of external resistance on electrogenesis, methanogenesis, and anode prokaryotic communities in microbial fuel cells. *Appl Environ Microbiol* 2011;77:564-71. DOI PubMed PMC
154. Jung S, Mench MM, Regan JM. Impedance characteristics and polarization behavior of a microbial fuel cell in response to short-term changes in medium pH. *Environ Sci Technol* 2011;45:9069-74. DOI PubMed